UNIVERSITÀ DEGLI STUDI DI MILANO

SCUOLA DI DOTTORATO IN MEDICINA MOLECOLARE

CICLO XXVIII

Anno Accademico 2014/2015

TESI DI DOTTORATO DI RICERCA

BIO10

TM9SF4: ROLE IN CANCER AND DEVELOPMENT

Dottorando: Marianna GRECO

Matricola N° R10175

Tutore: Prof.ssa Cristina BATTAGLIA

Co-tutore: Dott.ssa Ileana ZUCCHI

Direttore del dottorato: Ch.mo Prof. Mario CLERICI

SOMMARIO

Il gene tm9sf4 codifica per una proteina appartenente alla famiglia Transmembrane 9 Protein Superfamily, caratterizzata dalla presenza di nove domini trans-membrana e da un grado elevato di conservazione a livello evolutivo. In origine, essa è stata identificata in Dictyostelium e Drosophila come una proteina coinvolta nell'adesione cellulare e nella fagocitosi.
Studi più recenti hanno dimostrato che la proteina Tm9sf4 è espressa nelle cellule di melanoma derivate da metastasi ed è coinvolta in un processo chiamato "tumor cell cannibalism", che sembrerebbe essere una proprietà esclusiva delle cellule metastatiche. Le cellule tumorali sono in grado di fagocitare oltre a materiale amorfo, sia cellule tumorali sorelle, sia linfociti T diretti contro le cellule tumorali stesse. Pertanto, il cannibalismo consente alle cellule tumorali di rifuggire dal sistema immunitario dell'ospite, ne promuove la sopravvivenza in un ambiente ostile, caratterizzato da scarsità di nutrienti e ipossia, e consente loro di rimodellare la matrice extracellulare e di invaderla.
Nel nostro laboratorio, questo gene è stato messo in evidenza grazie alla linea cellulare LA7, che costituisce un modello di cellula staminale cancerosa (CSC, cancer stem cell) della ghiandola mammaria. I nostri dati preliminari dimostrano che il livello di espressione di tm9sf4 è maggiore nelle LA7 CSCs rispetto alla loro controparte differenziata. Inoltre, abbiamo osservato che la sotto-regolazione del gene induce le LA7 CSCs a trans-differenziare a cellule mesenchimali e provoca un aumento del livello di espressione di specifici marcatori di "epithelial to mesenchymal transition" (EMT), suggerendo che il gene potrebbe essere coinvolto in questa transizione.

Lo scopo di questo lavoro è l'identificazione della funzione di tm9sf4 nelle cellule normali e tumorali. Basandoci sulla considerazione che tutti i vertebrati mostrano conservazione nelle vie di trasduzione del segnale coinvolte in processi come la diramazione di tessuti che si differenziano in strutture tubulari, la migrazione cellulare e lo sprouting, abbiamo studiato il ruolo della proteina nello sviluppo embrionale di zebrafish (Danio rerio), che è stato recentemente indicato come un modello adatto allo studio delle malattie umane e dei processi associati all'oncogenesi.
Inoltre, il processo di EMT è stato proposto come il principale elemento guida sia per la morfogenesi durante lo sviluppo embrionale sia per la progressione dei tumori, coinvolgendo processi cellulari e cascate di segnale molto conservati.

L'espressione di tm9sf4 è stata analizzata mediante RT-PCR su RNA provenienti da embrioni a diversi stadi di sviluppo e tramite WISH (Whole Mount In Situ Hybridization), realizzando in seguito sezioni istologiche degli embrioni ibridati. Sono stati eseguiti esperimenti di genetica inversa (loss-of-function), iniettando embrioni allo stadio di 1-4 cellule con oligonucleotidi antisenso (morfolino), allo scopo di reprimere l'espressione di tm9sf4, utilizzando sia linee wild type sia la linea transgenica tg(gata1:dsRed)^{sd2}/tg(flk1:EGFP)^{S843}. Successivamente, è stata analizzata l'espressione di specifici marcatori del sistema nervoso centrale (CNS) e di EMT da parte degli embrioni precedentemente iniettati con i morfolino (morfanti), mediante ibridazione in situ e Real Time PCR.

Abbiamo dimostrato che durante lo sviluppo embrionale di zebrafish il gene è espresso in tutti gli stadi analizzati, da oocita a cinque giorni dopo la fecondazione (dpf, days post fertilization), indicando che l'espressione è sia materna sia zigotica. Inoltre, il gene è espresso principalmente nel CNS e, in seguito a sotto-regolazione della proteina, gli embrioni riportano necrosi a livello della testa e una ridotta definizione delle strutture cerebrali. L'analisi di espressione di marcatori di specifiche regioni del CNS ha evidenziato che tutte queste strutture sono formate nei morfanti, ma sono meno organizzate rispetto a quelle osservate negli embrioni di controllo. Inoltre, la sotto-regolazione della proteina induce un aumento del livello di espressione di fgf8, shha, wnt1 e una diminuzione dl livello di otx2. Questi risultati suggeriscono una funzione della proteina nello sviluppo del CNS.
D'altra parte, i morfanti a 24 ore dopo la fecondazione (hpf, hours post fertilization) riportano difetti nella regione denominata ICM (Intermediate Cell Mass), dove avvengono l'ematopoiesi primitiva e lo sviluppo dei vasi. A 48 hpf la circolazione è compromessa e si osservano edema cardiaco e stasi a livello della coda, dove si riscontrano difetti nei vasi intersomitici, che si formano per angiogenesi. E' importante evidenziare che l'angiogenesi rappresenta un modello per diversi processi biologici, tra cui la migrazione cellulare.
In seguito, abbiamo dimostrato che la sotto-regolazione di Tm9sf4 induce un aumento dei livelli di zeb2 e twist2 da parte dei morfanti a 24 hpf, suggerendo che la proteina potrebbe essere coinvolta nella soppressione di questi fattori, inibendo la repressione trascrizionale di E-caderina e promuovendo di conseguenza l'adesione cellulare. Questa ipotesi confermerebbe i precedenti studi, che attribuiscono a Tm9sf4 un ruolo nell'adesione cellulare. Inoltre, abbiamo osservato che il gene è maggiormente espresso nelle regioni periventricolari di diencefalo e mesencefalo, dove si trovano cellule in proliferazione, che sono in procinto di migrare e che vanno probabilmente incontro a EMT. Pertanto, abbiamo ipotizzato che la proteina potrebbe avere un ruolo nel reprimere il processo di EMT durante la neurulazione. Coerentemente con le nostre ipotesi, abbiamo dimostrato che la sotto-regolazione della proteina induce una diminuzione del livello di E-caderina in gastrulazione, promuovendo probabilmente la perdita dell'adesione cellulare.

In futuro, saranno condotti ulteriori studi, determinando in quali cellule del CNS il gene tm9sf4 è espresso e valutando l'effetto della sotto-regolazione della proteina sull'espressione di altri componenti della cascata che regola il processo di EMT, sia durante la gastrulazione, sia durante la neurulazione. Inoltre, sarà analizzata l'espressione di altri marcatori del CNS mediante ibridazione in situ, per stabilire nello specifico quali regioni sono compromesse in seguito a sotto-regolazione della proteina e, possibilmente, quali sono le vie di trasduzione del segnale coinvolte. Infine, saranno studiati più approfonditamente i problemi circolatori osservati nei nostri morfanti, sia mediante un approccio di genetica inversa con specifiche linee transgeniche, sia tramite l'analisi dell'espressione di marcatori cardiaci, allo scopo di stabilire se i problemi alla circolazione siano causati da difetti nello sviluppo del cuore, o se, al contrario, l'edema cardiaco sia provocato dai difetti morfologici osservati nei vasi intersomitici.

ABSTRACT

The tm9sf4 gene encodes a member of Transmembrane 9 Protein Superfamily, characterized by the presence of nine transmembrane domains and a high degree of evolutionary conservation. It was originally identified in Dictyostelium and Drosophila as a protein involved in cell adhesion and phagocytosis.
More recent studies reported that tm9sf4 is expressed in metastatic melanoma cells and it is involved in the process of tumor cell cannibalism, which might be unique to metastatic cells. Tumor cells indiscriminately phagocytize both sibling tumor cells and lymphocytes, in addition to amorphous material, thereby allowing tumor cells to escape from the immune response, promoting cell survival in a hostile microenvironment with low nutrient supplies and hypoxia conditions and allowing them to remodel and migrate through the extracellular matrix.

Tm9sf4 gene was brought to our attention by LA7 cells, which represent a cancer stem cell (CSC) model system. Our preliminary data showed that the expression level of tm9sf4 gene was higher in LA7 CSCs if compared to the differentiated counterpart. Tm9sf4 downregulation by RNA interference induced LA7 CSCs to trans-differentiate to mesenchymal-like cells and caused an increase of the expression level of EMT-associated markers, suggesting that the gene is involved in epithelial to mesenchymal transition (EMT).

The aim of my PhD project is to identify the function of tm9sf4 in normal and cancer cells. Based on the assumption that all vertebrates share common pathways involved in biological processes including morphogenesis-associated development of branched structures, cell migration and sprouting, we investigated Tm9sf4 protein function in zebrafish (Danio rerio), to further investigate its role in normal development. Zebrafish was recently proven to be a powerful model, to study not only human diseases, but also processes associated with oncogenesis. Additionally, EMT was suggested to be the major driver of both embryonic morphogenesis and tumor progression, involving highly conserved cellular processes and signaling pathways.

Tm9sf4 expression analyses were performed by both RT-PCR on RNA from embryos at different developmental stages and whole mount in situ hybridization (WISH). Histological sections of the stained embryos were performed. In addition, loss-of-function analyses were carried out by the injection of 1-4 cell stage embryos with antisense oligonucleotide morpholinos, using the zebrafish AB line (wild type) and the double transgenic line tg(gata1:dsRed)^{sd2}/tg(flk1:EGFP)^{S843}. The expression of specific brain markers and EMT-associated markers was assessed by WISH and Real Time PCR on embryos previously injected with morpholino oligos (morphants).

We demonstrated that during zebrafish embryogenesis the gene was expressed from oocytes to 5 days post fertilization (dpf), suggesting that the expression is both maternal and zygotic. Moreover, it was found to be mainly expressed in the central nervous system (CNS).
Following tm9sf4 downregulation, the embryos displayed head necrosis and an impaired brain compartmentation. Expression analysis of specific brain markers suggested that all of the targeted sub-structures were present in morphants, while

they were less well organized than in control embryos. Additionally, tm9sf4 downregulation induced an increase of the expression levels of fgf8, shha, wnt1 and a reduction of otx2 level. These findings suggested that the gene has a role in CNS development.
At 24 hours post fertilization (hpf) the morphants displayed tail bending and defects in the intermediate cell mass (ICM) region, where primitive hematopoiesis and vessel development occur. At 48 hpf the circulation was significantly impaired by protein downregulation, which caused cardiac edema and blood stasis in the tail, where morphological defects were detected in intersomitic vessels, which are formed by angiogenesis. It was suggested that angiogenesis represents a model for many core biological processes, including morphogenesis-related development of branched structures and cell migration, all of which are involved in the morphogenesis of many other organ systems.
We demonstrated that tm9sf4 downregulation induced an increase of zeb2 and twist2 expression levels by 24 hpf embryos, suggesting that tm9sf4 induces negative regulation of these factors, inhibiting E-cadherin transcriptional repression, resulting in its upregulation, which promotes cell-cell adhesion. This hypothesis is consistent with previous studies, which suggested a protein role in cell adhesion. Interestingly, we found the tm9sf4 gene to be most strongly expressed in the periventricular regions of the diencephalon and mesencephalon, where there are proliferating cells that are going to migrate and could undergo epithelial to mesenchymal transition. Hence, tm9sf4 could have a role in repressing EMT during zebrafish neurulation. We also demonstrated that during gastrulation Tm9sf4 protein downregulation induced a decrease of E-cadherin expression level, which could promote the loss of cell-cell adhesion.

In the near future we are going to further investigate the role of tm9sf4 in EMT, by determining in which specific CNS cells the tm9sf4 gene is expressed and by studying its effect on the expression of other components of the EMT signaling pathways, both in zebrafish gastrulation and neurulation.
WISH analysis of other brain markers is now in progress, to individuate the specific regions and, possibly, the pathways affected by Tm9sf4 protein downregulation.
Additionally, further investigations on circulation defects will be carried out, by both loss-of-function analyses on specific transgenic lines and cardiac markers expression studies, in order to establish whether the circulation problems are caused by defects in the heart development or rather the cardiac edema is due to the defective intersomitic vessels development.

INDEX

1. INTRODUCTION

1.1 From eating to feed to eating to defend

TM9SF4 was originally identified in *Dictyostelium discoideum* as a protein involved in cell adhesion and phagocytosis [1], [2]. The gene was named *phg1* and it encoded a member of *Transmembrane 9 Protein Superfamily*, or *nonaspanins*, characterized by a potential N-terminal signal sequence, followed by a large non-cytoplasmic domain and nine putative membrane-spanning segments. This family displays a high degree of evolutionary conservation.

In higher eukaryotes, phagocytic cells are essential players of the host defense against invading pathogens. The mechanisms involved in phagocytosis by *Dictyostelium* cells are very similar to those used by mammalian phagocytes. Phagocytosis involves adhesion of the phagocytic cell to the pathogen surface, and reorganization of the actin cytoskeleton to allow pathogen engulfment.

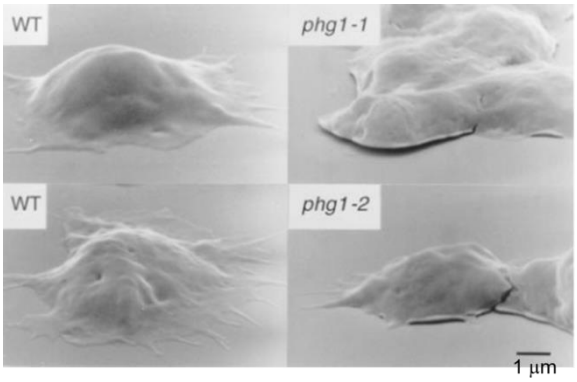

Figure 1 Scanning electron microscopy showing adhesion of wild-type (WT) and phg1 mutant *Dictyostelium* cells to their substrate. Scale bar 1 μm. Distinct mutations in *phg1* gene (right) cause a reduced ability to adhere to phagocytic substrates by *Dictyostelium* cells, with respect to wild type cells (left) [1].

It was shown that *phg1* mutant cells displayed a reduced ability to internalize particles, when incubated in the presence of latex beads. *Phg1* mutation did not affect fluid phase uptake, suggesting that the machinery responsible for formation of endocytic vacuoles was intact. On the other end, the ability of mutant cells to adhere to the phagocytic substrates was impaired (Figure 1) [1].

Moreover, *TM9SF4* protein was demonstrated to be involved in *Drosophila* immunity [3], [4]. In fact, *tm9sf4* is expressed in main immune tissues, such as gut, fat body cells, with the highest level in the plasmatocytes. In *Drosophila*, plasmatocytes are the most abundant type of circulating hemocytes and they are required for bacterial phagocytosis in innate response. On the other end, upon infection by parasites, plasmatocytes can attach to the invader and then signal to the lymph gland to promote the differentiation of another kind of hemocyte, called lamellocytes. *Drosophila* also has a sophisticated humoral response, which includes the synthesis of antimicrobial peptides by fat body cells, under control of Toll and Immunodeficiency pathways, which are stimulated by Gram-negative (G-) and Gram-positive (G+) bacteria, respectively. Mutant flies that did not produce a functional protein were shown to be sensitive to G- pathogenic bacteria. In this flies Toll pathway was not affected; in contrast, phagocytosis of G- bacteria by mutant plasmatocytes was two times less efficient with respect to wild type cells. The sensitivity of the mutant flies to G- bacteria was supposed to be due to the impaired ability of plasmatocytes to adhere to the pathogen surface, because of the defects in actin organization. Confocal analysis of the chromatin network showed that plasmatocytes from mutant flies had heterogeneous sizes and morphology and displayed disorganized long actin spikes and punctate actin accumulation [3].

1.2 Tumor cell cannibalism

In humans, four *tm9sf* genes have been identified. *Tm9sf4* is characterized by a high degree of evolutionary conservation, suggesting that *Dictyostelium, Drosophila* and human proteins may have similar functions.
More recent studies suggested that human *TM9SF4* protein is involved in the process of tumor cell cannibalism [2], [5], [6].
Cannibal behaving tumor cells were identified more than a century ago (*Steinhaus, 1891; Stroebe, 1982*) in malignant tumors with different histology, including breast carcinoma, hematological malignancies, bladder cancer, medulloblastoma, gastric adenocarcinoma, melanoma and skin carcinomas. They were described as tumor cells containing engulfed material of different origin in large vacuoles that push the nucleus to the cell periphery. Figure 2 shows a human melanoma cell with a large vacuole containing an apparently live neighboring cell, which pushes the melanoma cell nucleus to the periphery (right) and a melanoma cell containing cell remnants in its internal vacuole (left) [7]. This behavior might be a hallmark of metastatic cells, since it was not observed in cells derived from primary tumors [8][i].

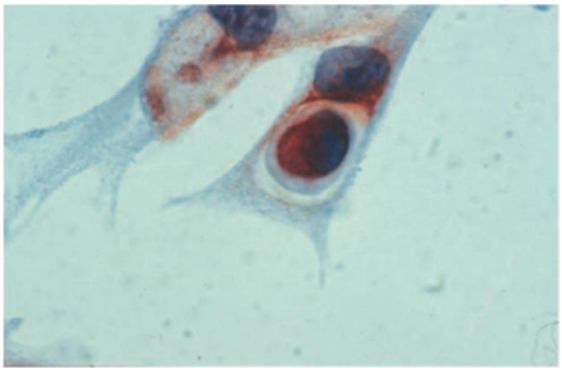

Figure 2 Immunocytochemistry depicting two human melanoma cells in different stages of the cannibalism process. Lysosomal membrane protein-1 (LAMP-1) staining [7].

Tumor cells indiscriminately internalize amorphous material as well as apoptotic and healthy cells; in particular, they phagocytose both sibling tumor cells and lymphocytes that should kill them. In addition, it has been demonstrated that the percentage of surviving tumor cells increases, in the absence of serum or amino acids, when the melanoma cells are co-cultured in the presence of T-cells [5]. Hence, the main functions of this behavior are to feed upon other cells, to nibble the extracellular matrix and to escape from the specific immune response. These characteristics are peculiar of highly invasive and metastatic tumor cells, because they promote cell survival in a hostile microenvironment, with low nutrient supplies and hypoxia conditions, and allow them to remodel and migrate through the extracellular matrix.

This process is different from the typical phagocytosis, where the engulfment is preceded by the formation of ruffles and pseudopods, embracing the external body. In this case, the internalization occurs through a sequence of events, including early interaction between the two cells (Figure 3, E-F), tumor cell invagination (Figure 3, G-H) and entrapment of lymphocyte within the melanoma cell (Figure 3, I-J) [5]. In particular, this process requires big caveolar-like vacuoles (Figure 4) in the site of the interaction between the tumor cell and the lymphocyte and a link between caveolin 1 expressing vacuoles and the actin cytoskeleton. The connection may be provided by the actin-linker molecule ezrin, which belongs to the ERM actin binding protein family (ERM, Ezrin, Radixin, Moesin) [5]. Furthermore, the pH of vesicles is lower in metastatic melanoma cells respect to primary melanoma cells. The acidic environment activates proteolytic enzymes, like cathepsin B, which is required for cannibalistic activity [2], [5].

Each of the components of the cannibal framework may represent specific tumor targets for future new strategies against cancer.

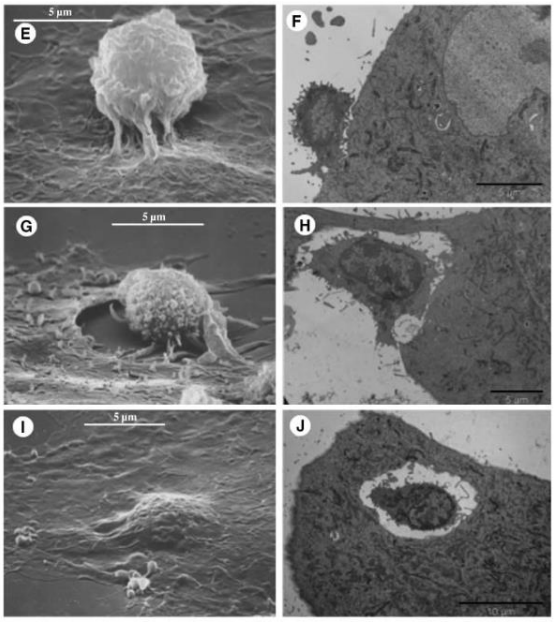

Figure 3 Scanning electron microscopy (SEM), on the left, and transition electron microscopy (TEM) analysis, on the right, after co-culture of metastatic melanoma cell monolayer with live autologous tumor-specifc $CD8^+$ T-cells, recognizing the melanoma antigen MART-1 [5].

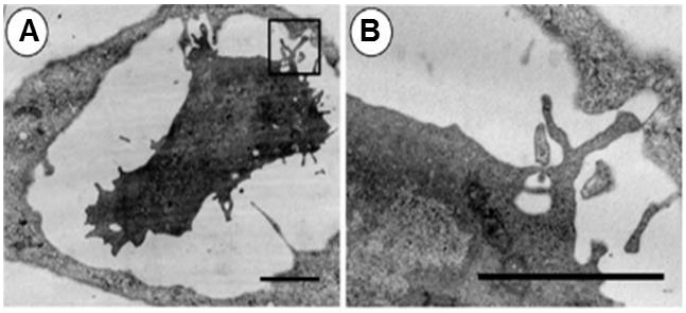

Figure 4 TEM analysis of an internalized lymphocyte undergoing degeneration [5].

For which concerns the role of *tm9sf4* in this process, it's important to notice that the gene is expressed in metastatic melanoma cells, having cannibalistic activity, but not in primary melanoma cells, which do not display this behavior. The protein is localized in early endosomes. It is involved in phagocytic and cannibal activity of metastatic melanoma cells,

since *tm9sf4* knock-down by RNA interference significantly impairs the phagocytic activity of these cells against yeast and the cannibal activity against autologous lymphocytes. Furthermore, *tm9sf4* silencing induces an increase of intravesicular pH of melanoma cells and a decrease of cytosolic pH, suggesting a protein role as an ion channel component or an ion channel regulating element, involved in the control of intracellular vesicle pH [2].

1.3 LA7: a cancer stem cell model system

Tm9sf4 gene was brought to our attention by LA7 cell line, which represents a model of mammary gland cancer stem cell (CSC), which allows us to study the dynamics of tumor formation at the single cell level and to investigate certain aspects of normal mammary gland development. LA7 cells, characterized by a polygonal epithelial morphology, were isolated by Renato Dulbecco from a chemically induced rat adenocarcinoma [9].

According to cancer stem cell hypothesis, tumors are derived from mutated stem cells that have retained the properties of self-renewal and differentiation potential or from progenitors that have regained these characteristics. These kinds of tumor contain a hierarchical population of cells, composed by a majority of differentiated cells and a small number of tumor initiating cells. Since mammary tumors have been demonstrated to be often clonal in origin, they are supposed to be generated from a single mutated stem cell [10].

In our laboratory, it has been shown that LA7 cells can be propagated indefinitely both in monolayer and in suspension culture. In non-adherent conditions LA7 mammospheres could be regenerated indefinitely from cells derived from previously dissociated mammospheres. In these conditions

LA7 cells maintain their undifferentiated status, since they do not express mammary gland lineage specific cell markers.

The mammary gland is composed of stem cells, which possess the capacity of indefinite self-renewing, lineage-committed progenitor cells, that have lost this capacity, but still possess proliferation and differentiation potential, and terminally differentiated cells, belonging to three cell lineages: luminal, alveolar and myoepithelial cells. LA7 stem cells confluent monolayer cultures, treated with differentiation inducers, are able to form domes, which are structures reminding mammary gland alveoli. A single mammosphere seeded onto collagen-coated dishes can give origin to branched-like structures, reminiscent of tubules, that are composed of myo-epithelial and luminal cells, expressing cytokeratin 14 (K14) and cytokeratin 18 (K18) respectively. When treated with lactogenic hormones, LA7 mammosphere-derived outgrowths produce milk proteins such as β-casein, which is a marker specific for functional terminally differentiated alveolar cells [11].

Hence, *in vitro*, LA7 cells have the ability to serially regenerate mammospheres in long-term non adherent cultures, the differentiation potential to generate all the cell lineages of the mammary gland and to develop tubular structures that recapitulate, morphologically and functionally, the ductal-alveolar-like architecture of the mammary tree (Figure 5) [11], [12].

In vivo, when injected at the single cell level in nonobese diabetic severe combined immunodeficient (NOD-SCID) immunocompromised mice, they are able to generate tumors with a heterogeneous morphology and containing cells with different ability to self-renewing and three dimensional organotypic growths. The tumor heterogeneity is the result of the clonal expansion of a single LA7 cell in all the cell lineages of the tissue of origin. [11] (Figure 6).

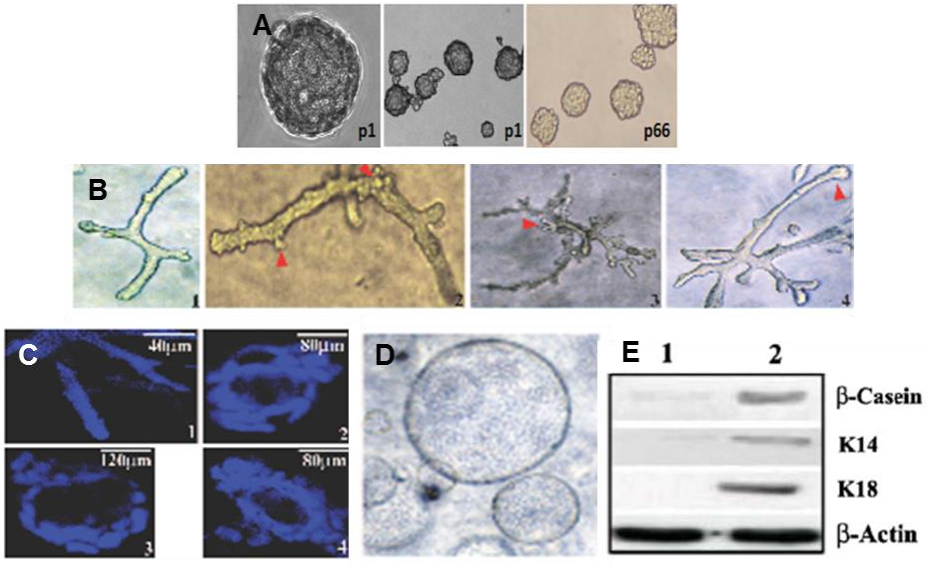

Figure 5 LA7 cells *in vitro* properties. (A) Self-renewing mammospheres generated by LA7 cells. (B) Tubuli generated from a single LA7 cell in collagen. (C) Confocal microscopy of tubular elongated structures and cross-sections of hollow tubuli (staining with Hoechst nuclear dye). (D) Cyst-like structures generated by LA7 cells in matrigel. (E) Expression of mammary gland specific markers by undifferentiated cells (lane 1) and by cells collected from LA7-derived tubules (lane 2).

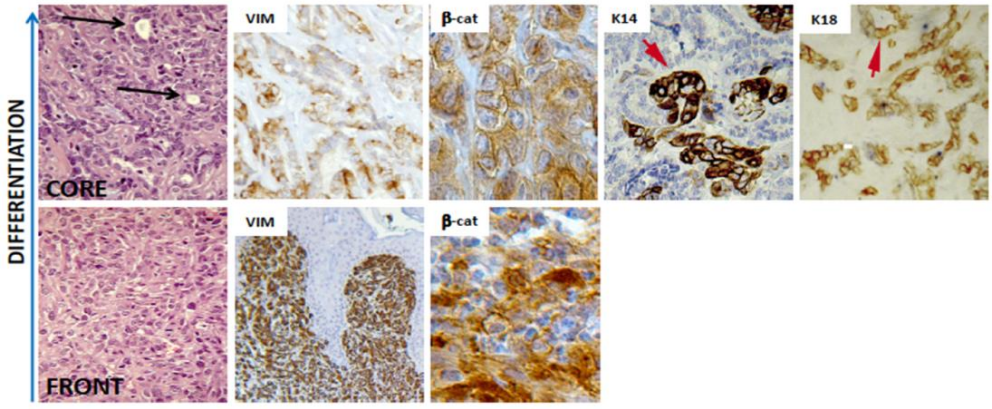

Figure 6 Histology and marker expression of the tumor generated from a single LA7 cell. The invasive front of the tumor expresses EMT markers (bottom), whereas the tumor core displays differentiation markers and reduced vimentin and β-catenin (top).

In particular, the tumor contains highly proliferating cells, expressing Ki67, and terminal differentiated cells, expressing K18 or K14. The cells expressing K14 or K18 are not randomly dispersed, but they are organized in structures reminding tubuli typical of the tissue of origin.

After tumor dissection, three different populations of LA7-derived cells could be identified, based on their morphology: a population having epithelial polygonal morphology, another one having fibroblast-like elongated morphology, called LA7 Elongated (LA7E), and a population of mesenchyme-like cells. The last one displays a limited expansion capacity *ex vivo* and it is not able to generate spheres and organotypic structures. In contrast, polygonal cells are cancer stem cells with the property of self-renewing, while LA7 elongated cells are lineage-committed progenitor cells. These two cell types have different ability to serially regenerate mammospheres and to generate three-dimensional structures *in vitro* and they differ for the capacity to develop and to sustain tumors *in vivo* [13].

A microarray-based expression analysis showed that *tm9sf4* was one of the top 50 genes found to be differentially expressed in LA7 CSCs respect to LA7 Elongated cells with high significance (unpublished data). This result was validated by real time PCR, which confirmed that *tm9sf4* expression level was higher in LA7 CSCs, if compared to the differentiated counterpart (Figure 7). Therefore, loss-of-function experiments were performed on LA7 CSCs by RNA interference, demonstrating that *tm9sf4* downregulation caused changes in LA7 CSCs morphology, inducing them to trans-differentiate to mesenchymal-like cells (Figure 8, unpublished data).

Hence, we hypothesized that the changes in cell morphology observed in LA7 CSCs following siRNA treatment were associated with an epithelial to mesenchymal transition (EMT) process.

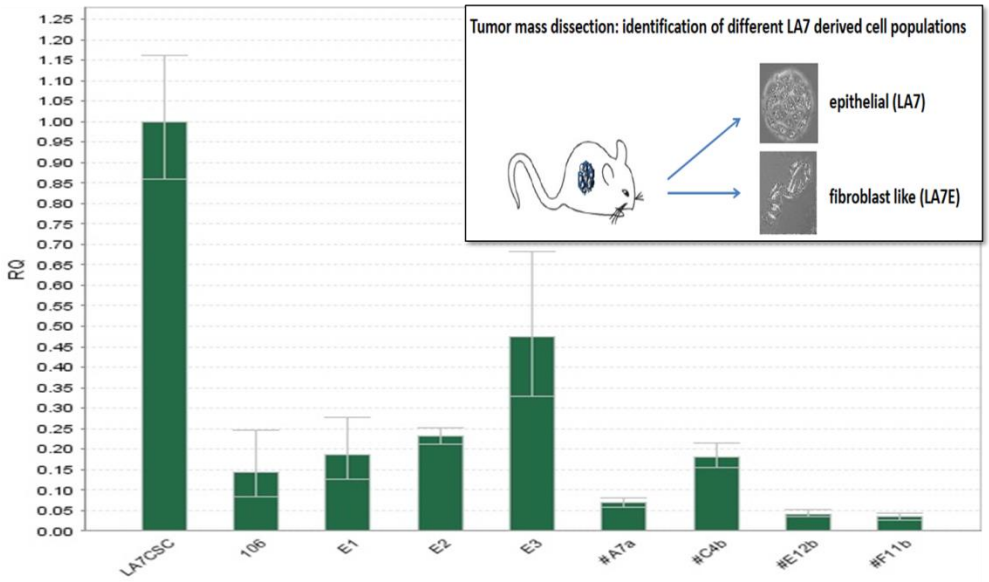

Figure 7 Distinct cell populations derived from tumor dissection (top). Expression level of *tm9sf4* (bottom) in LA7 CSCs compared to LA7 progeny, measured by qRT-PCR (endogenous control HPRT).

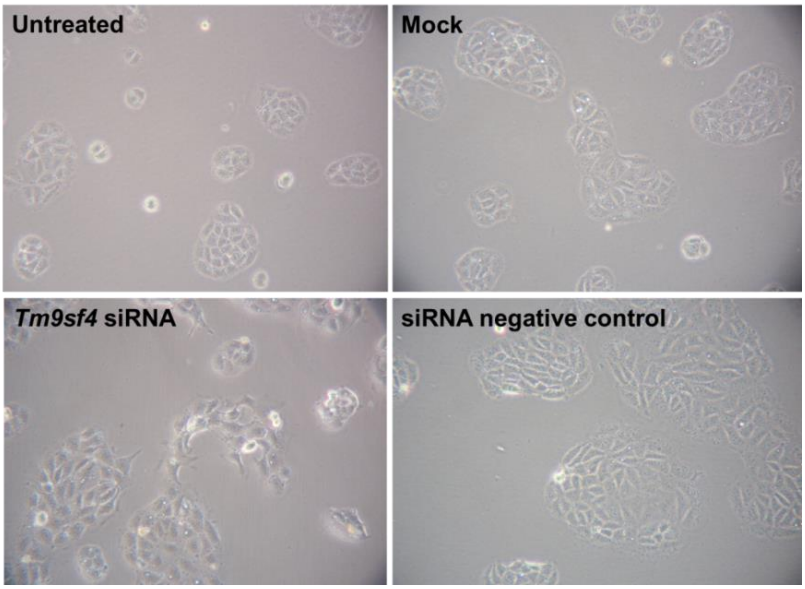

Figure 8 Loss-of-function analysis on LA7 CSCs.

To answer this question, we assessed the expression level of specific EMT markers (*twist1, twist2, zeb2)*, by qRT-PCR, in LA7 CSCs, after *tm9sf4* downregulation. All the markers analyzed resulted upregulated in *tm9sf4* siRNA treated cells, with respect to control cells (Figure 9, unpublished data).

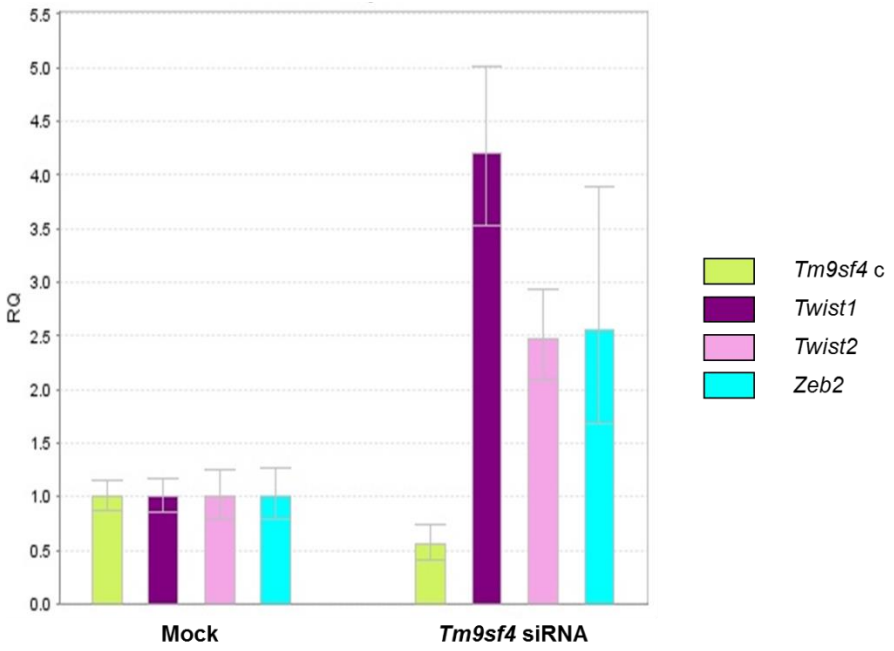

Figure 9 Analysis of EMT marker expression, performed by Real time PCR assay on LA7 cells treated with 25 nM *tm9sf4* siRNA for 48 hours compared to mock control cells, treated with just the transfection agent InterferIN.

1.4 Danio rerio as a model system

Since zebrafish (*Danio rerio*) was proven to be a powerful model, to study human diseases and processes associated with oncogenesis, we decided to investigate the role of *Tm9sf4* protein in zebrafish embryonic development [14]–[18].

Zebrafish is a freshwater tropical fish, native to the streams of the southeastern Himalayan region and it is found in India, Pakistan, Bangladesh, Nepal, and Burma (Figure 10). The name derives from the blue stripes on the side of the body, which extend to the end of the caudal fin. The zebrafish can grow up to 6.4 cm. They are characterized by a torpedo shape. Females have a larger belly and they exhibit a small genital papilla in front of the anal fin origin. Its lifespan in captivity is around two to three years, although in ideal conditions, it may be extended to over five years.

Figure 10 Zebrafish female (top) and male (bottom).

Zebrafish have a fully mapped genome, which has significant homology with the human genome, including noncoding regions, suggesting that numerous genes involved in human diseases have conserved sequence and function in zebrafish.

They are cheap and easy to house and care of, due to their small size and the relatively simple environment conditions required.

The impact of any genetic mutation or drug treatment and the early developmental processes are easy to see, because the larvae are transparent up to 7 days post fertilization (dpf); in addition, this can be extended to up to 9–14 dpf with the addition of melanocyte inhibitors. Moreover, the availability of transparent adult zebrafish, such as the Casper line, adds new imaging possibilities [19]. The transparency of zebrafish,

associated to sophisticated fluorescent technologies, permits to mark signaling proteins or cellular entities, allowing for the imaging of biological and disease processes. Zebrafish are highly fecund: a pair of zebrafish produces over 100 embryos per clutch, which are usable for larval experiments. The embryos breed and develop very quickly: in fact, an adult zebrafish develops in 3 months. The first cellular division occurs after approximately 45 minutes. During the first 8 hours of development, it is possible to observe the embryonic cells to cleave on the top of the yolk, followed by epiboly, in which cells move down and establish the anterior-posterior axis. The formation of different organ systems can be followed under the microscope. At 24 hours post fertilization (hpf), the embryo displays well defined morphological characteristics: for example, it shares a vascular system and a well-organized nervous system; moreover, eyes, otolites, somites, pronephric ducts and blood cells precursors can be observed. At 48 hpf, also a cardiac pump and blood circulation can be visualized. The developing gastrointestinal system can be detected using specific molecular markers, whereas it will be possible to analyze its morphology at 5 dpf. Furthermore, a liver with histology similar to mammals is detectable.

In addition, knock-down (morpholino injection) and forward genetic (mutagenesis, transgenic lines) techniques are well established and commonly used to manipulate and characterize zebrafish gene function. The embryos can be easily injected at the 1-4 cell stage with antisense morpholino oligonucleotides, targeting specific gene transcripts, to perform loss-of-function studies.

Additionally, since zebrafish is a vertebrate, it has many features commonly found in mammals, including an innate immune system, composed of neutrophils, NK cells, and monocytes/macrophages, that become functional by 48 hpf [20] and an adaptive immune system that is fully functional at 4–6

weeks post fertilization [15]. The adaptive immune system, as in mammals, includes T-cells and B-cells that undergo Rag-dependent V(D)J-recombination.

A wide range of larval and adult zebrafish models that recapitulate human diseases is available, including different branches of pathology, such as wound healing, gastrointestinal disease, microbe-host interactions, genetic diseases and drug screens [21].

Zebrafish is particularly useful for the study of hematopoiesis [22]. Blood circulation begins approximately at 24 hpf and the number and morphology of circulating cells are visible under a microscope. The hematopoietic process is conserved throughout vertebrate evolution: in fact, many mouse and human homologues of blood specific genes have been cloned in zebrafish (*scl, lmo-2, gata-1, and c-myb*). More than 50 mutants with hematopoietic defects have been identified [16].

Furthermore, zebrafish can be used to study cardiovascular disorders. The zebrafish embryonic heart resembles the heart of a human embryo at three weeks of gestation. It is divided into atrial and ventricular chambers and it is lined by endocardium, with cardiac valves forming at the chambers boundaries. The heart starts to beat at approximately at 22 hpf with a peristaltic wave and, by 36 hpf, the beating is generated by coordinate contractions of atrium and ventricle. Studying the heart in zebrafish is particularly convenient, because the heart function can be assessed visually; moreover, the fish, unlike mouse, is not dependent from blood circulation for survival in early development [16].

Zebrafish represent a useful model system for kidney disorders. The pronephric kidney is composed by two nephrons with fused glomeruli and bilateral pronephric ducts. Zebrafish kidney development and function resemble for many aspects higher vertebrates kidney [23].

Finally, *D. rerio* has been proposed to be an ideal vertebrate system in which to model cancer [14]. Teleosts develop a wide variety of benign and malignant tumors in virtually all organs, with a histology resembling that of human tumors. Cell-cycle genes, tumor suppressors and oncogenes are conserved between human and zebrafish genome sequence. Hence, mutagenesis screens targeted to these pathways could be designed, to analyze the resulting phenotypes in the developing embryos. This system also provides a way to check if a mutation causing an embryonic phenotype is related to a cancer predisposition in adults. Zebrafish system can be used for chemical genetic screens, to identify drugs active in multicellular organisms [24]. In fact, embryos exhibit many features of cancer, like rapidly dividing cells, extensive apoptosis and angiogenesis. Screens for compounds that affect these properties could identify drugs potentially useful for cancer treatment. Transgenic lines could be used to express oncogenes or to follow gene expression through the use of GFP and rapid short-term analysis of gene function could be carried out using morpholinos that are often successfully used to phenocopy mutants.

Interestingly, it has been suggested that all vertebrates share common pathways involved in processes like development of branched structures, cell migration and neurogenesis [25]. Our hypothesis is that *tm9sf4* could be involved in one of these pathways. Hence, studying the protein function in this model may help us to understand its role in normal embryonic development and in tumorigenesis.

1.5 Transmembrane 9 protein superfamily in zebrafish

In zebrafish five genes belonging to transmembrane 9 protein superfamily have been identified: *tm9sf1* (NM_001003550), *tm9sf2* (NM_212728), *tm9sf3* (BC046021), *tm9sf4* (NM_200510) and *tm9sf5* (XP_686483) [26].

Splice variants could be found in databanks for all the human genes, in most cases in the N-terminal variable part. In particular, four variants were reported for human *tm9sf4*, while in zebrafish no splice variants were identified.

Zebrafish *tm9sf4* gene is located on chromosome 23 and it is composed by 16 exons, while the human gene resides on chromosome 20 and it includes 18 exons. *Tm9sf* genes were found to be ubiquitously expressed in tissues of adult zebrafish. During embryonic development, the expression of all *tm9sf* genes was detected from fertilization up to 4 dpf [26].

Bioinformatics analysis of 80 Tm9sf protein sequences from yeast, plants and animals showed that the protein have a conserved structure. Based on preliminary bioinformatics analyses, zebrafish Tm9sf4 protein was predicted to be composed by 9 transmembrane regions, a large variable region facing the non-cytoplasmic side, a C-terminal end orientated to the cytoplasmic side. At the N-terminus, a small cytoplasmic N-terminal part or another transmembrane region could be present [26] (Figure 11).

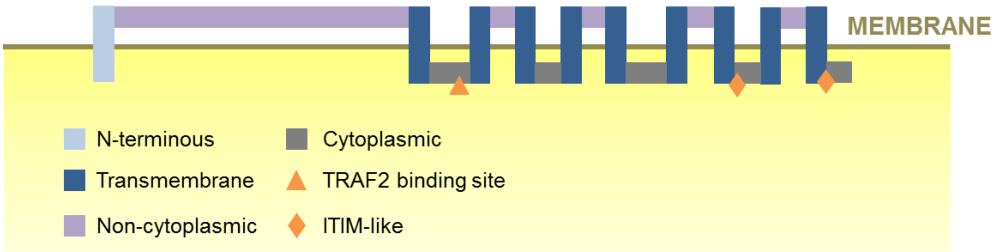

Figure 11 Prediction of the Tm9sf4 protein membrane topology

Two ITIM-like (Immunoreceptor Tyrosine-based Inhibition Motif) sequences could be present at the C-terminal end, close to transmembrane regions 7 and 9, respectively. A putative TRAF-2 (Tumor Necrosis Factor Receptor-Associated Factor 2) binding site is present between transmembrane regions 1 and 2. These domains are conserved in all Tm9sf proteins [26]. ITIMs have been found in a large number of immune receptors that were

shown to negatively regulate cellular processes including endocytosis, phagocytosis and cell adhesion. When ITIM-containing receptors are engaged, they become tyrosine phosphorylated and then they transmit inhibitory signals by binding and activating SH2 (Src homology domain) containing phosphatases. In many cases the target is *Vav1*, a guanine nucleotide exchange factor, which participates in several processes requiring cytoskeletal reorganization. Hence, the presence of ITIM motifs could place Tm9sf proteins in signal transduction pathways that may regulate processes such as adhesion and phagocytosis. On the other end, recently, ITIM and ITIM-like motifs have also been detected in proteins that are not directly involved in immunity, such as G-proteins in which it mediates apoptosis.

TRAF proteins are signal transducers for members of the TNF receptor family, even if TRAF signaling is not restricted to these receptors. TNF receptor-mediated TRAF2 signaling may lead to cell proliferation, cell activation and cytokine secretion. TRAF2 has also a role in cell differentiation or maturation in B cells, osteoclasts and macrophages. As TRAF2 protein is ubiquitous, a role of this protein in not direct immune functions may also be expected. TRAF2 could be involved in the induction of autophagy in the unfolded protein response (UPR), where TRAF2 is recruited by the endoplasmic reticulum serine/threonine kinase IRE1.

However, this prediction suggests that Tm9sf proteins could be involved in zebrafish immunity and it is consistent with the previous works, which shown protein involvement in the innate immunity of *Drosophila* and *Dictyostelium* [1], [3], [4].

Despite of this, the expression of *tm9sf* genes was not affected by incubation of the embryos with PAMPs (Pathogen Associated Molecular Patterns), such as LPS, CpG, poly I:C, at any concentration or length of exposure [26]. Therefore, the role of Tm9sf4 protein in zebrafish immune

system could be related to signaling. According to this hypothesis, it was suggested that Tm9sf proteins may transduce signals from PAMPs [26].

1.6 Epithelial to mesenchymal transition

Most adult tissues develop from a series of conversions of epithelial cells to mesenchymal cells, through the epithelial to mesenchymal transition (EMT) and the reverse process, mesenchymal to epithelial transition (MET). Several rounds of EMT and MET are required for final cell differentiation and the development of the complex structure of organs (primary, secondary, tertiary EMT). Primary EMT includes the formation of mesoderm from the primitive ectoderm and the repositioning of the three primary germ layers, as well as the definition of the anteroposterior and dorsoventral axes in the developing embryo, by mesendodermal progenitors undergoing EMT during gastrulation, and, successively, the formation of dorsal neural tube by neural crest delamination. Secondary EMT involves early mesodermal cells (axial, paraxial, intermediate, lateral plate cells), which condense into transient secondary epithelial structures (notochord, somites, somatopleure and splanchnopleure respectively), that will undergo EMT, leading to the generation of mesenchymal cells, that differentiate into specific cell types: for instance, endodermal tissues, including pancreas bud and liver diverticulum, undergo the dissociation of endocrine cells and hepatoblasts from their epithelial primordia. An example of tertiary EMT occurs in the heart during the formation of cushion mesenchyme, which is the precursor of cardiac valves, from the atrioventricular canal or the outflow tract.

Epithelial cells establish close contact with their neighbors and an apicobasal axis of polarity. They maintain global communication through specialized junction structures and they remain separated from adjacent

tissues by the basal lamina. In contrast, mesenchymal cells are dispersed in a three-dimensional extracellular matrix and comprise connective tissues adjacent to epithelia. In general, the EMT process involves morphological changes of epithelial cells, the loss of cell-cell adhesion and cell polarity, in addition to the acquisition of migratory and invasive properties. Furthermore, the expression of specific proteins occurs: cell-cell junction proteins and cytokeratin intermediate filaments are replaced by vimentin filaments and fibronectin.

Mesoderm formation and neural crest delamination represent the key embryonic EMT programs. Some of the most important elements involved in this process are conserved through evolution [27]. The genetic pathways governing gastrulation in amniotes, which are substantially maintained in zebrafish, are shown in figure 12 [27].

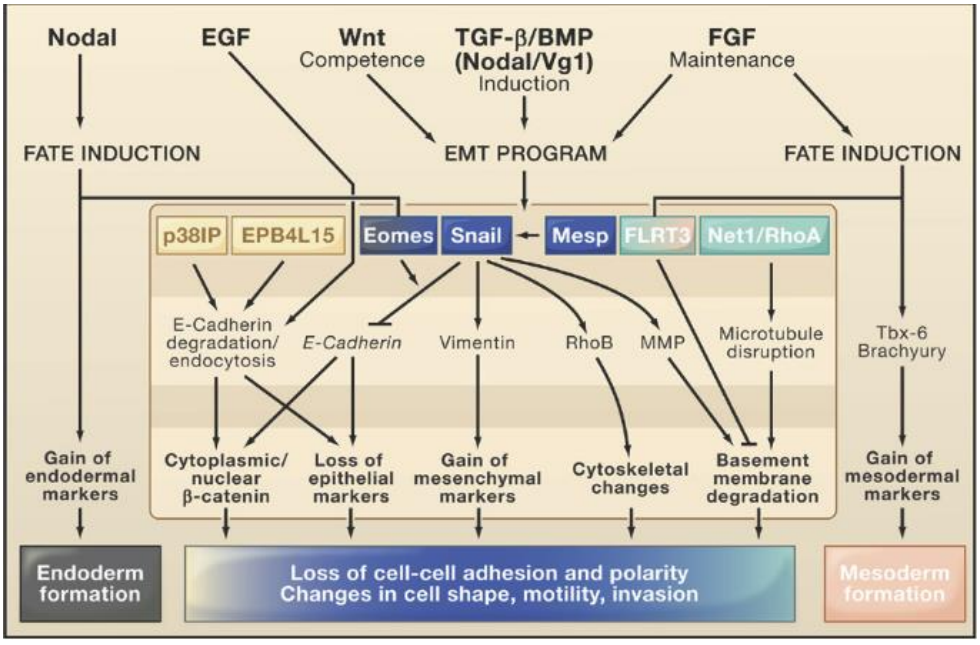

Figure 12 Genetic pathways controlling gastrulation in amniotes [27].

In early development, at the onset of gastrulation, activation of canonical *Wnt* (Wingless-type MMTV integration site family) signaling leads to the formation of the primitive streak or blastopore in the posterior part of the embryo, which is the region where cells involute or ingress and that establish a bilateral symmetry in most vertebrates. In zebrafish, the blastopore is not present and the cells involute at the blastoderm margin. In this region, convergence movements produce a local accumulation of cells, known as the embryonic shield in zebrafish (node in mammals), which is an organizing center, regulating cell movements and specification [28]. The formation of this structure is promoted by β-catenin, which, in turn, is regulated by *Wnt* and is transported in the dorsal part of the embryo by a maternal program of microtubule dependent transport, activating transcription factors and secreted signals in dorsal blastomers. Later, members of TGF-β superfamily (i.e. *Nodal*) mark the beginning of gastrulation, in both zebrafish and Xenopus. Nodal signaling and FGF (Fibroblast Growth Factor) family control the specification of mesoderm in all vertebrates. Members of TGF-β superfamily induce *Snail1* and *Snail2* (*SNAI1* and *SNAI2* in humans), which are E-cadherin repressors and control cell-cell adhesion, cell shape and motility. In addition, they are essential for EMT and mesodermal cells migration. FGF signaling is required to maintain their expression and for gastrulation to proceed [29]. The cell delamination is allowed by microtubule disruption and basal membrane breakdown, induced by *Net1* (RhoGEF protein), which inhibits *RhoA* in the blastopore [30]. On the other end, *FLRT3* maintains the basal membrane integrity in other areas [31].

In particular, zebrafish gastrulation involves a set of movements: blastoderm expansion around the syncytial yolk cell, which is associated with its thinning (epiboly), the migration of mesodermal and endodermal precursors from the blastula surface beneath the ectodermal layer, forming

an internal layer, the so called hypoblast (ingression), the conversion movements narrowing embryonic tissues mediolaterally and extension movements elongating tissues along the anteroposterior axis (Figure 13) [28]. Finally, deep cell layer (DEL) cells, adjacent to the blastoderm margin, become lineage restricted.

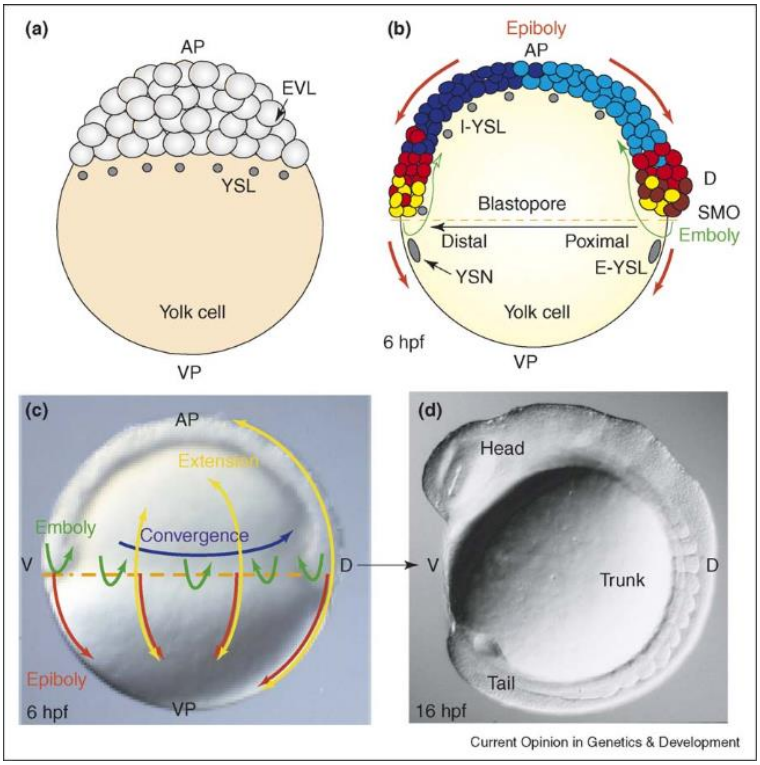

Figure 13 Gastrulation movements in zebrafish. (a) Midblastula stage. (b, c) Gastrulation. (d) 16 hpf embryo. Abbreviations: AP, animal pole; D, dorsal; E-YSL, external yolk syncytial layer; I-YSL, internal YSL; SMO, Spemann-Mangold organizer; V, ventral; VP, vegetal pole; YSN, yolk syncytial nuclei. Color code: red, mesoderm; dark red, prechordal mesoderm; yellow, endoderm; light blue, non-neural ectoderm; dark blue, neural ectoderm. The black arrow indicates the proximodistal blastopore axis [28].

Interestingly, many genes controlling these cell movements are involved in cell adhesion [28]. Moreover, it has been recently demonstrated that E-cadherin (*cdh1*) is involved in epiboly, convergence and extension

movements in zebrafish [32], [33]. In particular, E-cadherin-mediated adhesion between enveloping layer (EVL) and DEL cells could play a role in epiboly.

Furthermore, in the embryonic shield, prechordal mesendodermal cells internalize by synchronized ingression and successively they migrate towards the animal pole [32]. Activation of *stat3* downstream to β–catenin is essential for convergence and extension movements in the axial tissues [33]. The main effector of *stat3* is *liv1*, a zebrafish homolog of a breast cancer-associated zinc transporter, which promotes the nuclear localization of *snail*, a transcription factor that negatively regulates E-cadherin expression. It has been proposed that *liv1* promotes EMT in prechordal mesendodermal cells [34].

Wnt non-canonical signaling, mediated by *wnt11,* is also required for this process and it has been proposed to modulate cell adhesion by regulating E-cadherin activity [35]. Moreover, the T-box gene *notail,* the zebrafish homolog of *Brachyury*, and *wnt11* are required for the migration of the notochord precursors [36], [37].

Despite the heterogeneity of the mechanisms involved in gastrulation movements, E-cadherin has been shown to be essential for different cell behaviors underlying these processes [28]. The role of E-cadherin is conserved through evolution. It is unclear how E-cadherin function is regulated in terms of transcription, translation and protein activity. Since the gastrulation events occur very rapidly, many pathways should cooperate to ensure a dynamic and rapid regulation of E-cadherin.

After gastrulation the epidermal and neural (neuroectoderm) territories are progressively defined and the neural crest forms from ectoderm at the boundary between these two territories, characterized by an intermediate BMP (Bone Morphogenic Protein) signaling. BMP proteins belong to TGF-β superfamily. Neural crest is a transient population of embryonic progenitors,

which constitute the dorsal midline of the early neural tube and have the ability to undergo EMT and migrate as single cells over extraordinarily long distances. After migration they generate a wide variety of derivatives, including, among others, craniofacial structures, most of the peripheral nervous system, some endocrine cells and melanocytes. Canonical *Wnt* signaling is important for neural crest precursors induction and stabilization, whereas non-canonical *Wnt* signaling is required for neural crest migration [38]. One critical component of neural crest migration is the extracellular matrix: high levels of fibronectin and hyaluronan appear in the neural crest area just before migration.

In both developmental processes and carcinoma progression and metastasis, functional loss of E-cadherin in epithelial cells is considered a hallmark of EMT. Therefore, a pivotal importance represents the understanding of pathways through which E-cadherin is regulated. A wide range of transcription factors, including *Snail* and *ZEB*, are able to repress E-cadherin transcription by directly binding E-box elements present on its promoter [39]–[41]. Other factors, including the bHLH factor *Twist*, regulate E-cadherin indirectly [42], [43]. Interestingly, most of these factors are involved in various EMT processes, occurring both during embryogenesis and in tumor malignancy and metastatization.

2. AIMS

The aim of my PhD project is the identification of Tm9sf4 protein function in normal and cancer cells, in particular in mammary gland stem cell maintenance and in tumor initiation and progression.

Based on the assumption that all vertebrates share common pathways involved in many important biological processes, including tissue branching, cell migration, sprouting and neurogenesis [25], Zebrafish (*Danio rerio*) was used as an *in vivo* model system, to investigate Tm9sf4 protein function in embryonic development.

D. rerio was recently proven to be a powerful model to study not only human diseases, but also processes associated with oncogenesis. Since zebrafish is a vertebrate organism, it shares genetic similarity to humans and, to date, all proteins studied for their involvement in many human diseases have conserved sequences and functions in fish and mammals. Moreover, the zebrafish are easy to house and care for. The impact of any genetic mutation or drug treatment is easy to visualize under microscope, because the embryos are completely transparent. They produce a large number of eggs per mating and the embryos breed and develop very quickly.

Interestingly, most of the processes associated with EMT are conserved for many aspects in zebrafish embryonic development and human tumor progression [27], [44]. Our hypothesis is that *tm9sf4* is involved in one of these pathways. In particular, it could have a role in the regulation of EMT in various embryonic tissues and in tumor progression. Therefore, studying Tm9sf4 protein function in zebrafish may help us to understand its role in normal embryonic development and in tumorigenesis.

3. MATHERIALS AND METHODS

3.1 Zebrafish maintenance

Adult zebrafish were kept at 28 °C in a cabinet equipped with fish tanks (Figure 14), each one containing 3-5 liters of fish water, composed by a solution of 34 g of Instant Ocean Sea Salt per liter of dH_2O, further diluted 1:200 in dH_2O. They were fed three times per day with *Artemia Salina* and dried flake food. The light/dark cycle was 14/10 hours. Males and females were kept in separate tanks until mating.

In order to permit reproduction, a male and a female were combined, after the dark period, in 1 liter tanks, equipped with a mesh, to prevent adults from cannibalism and allow fertilized eggs to settle to the bottom. Zebrafish embryos obtained from natural spawning were collected in Petri dishes containing fish water, added with 0.01% methylene blue, to prevent fungal growth, and maintained at 28 °C until they reached the desired developmental stage, according to established techniques [Westerfield, M. 1995, The Zebrafish Book. A Guide for the Laboratory Use of Zebrafish (Danio rerio), 3rd Edition. Eugene, OR, University of Oregon Press, 385]. The embryos were staged according to morphological criteria [45].

Beginning from 24 hpf they were cultured in fish water containing 0.003% PTU (1-phenyl-2-thiourea; SIGMA) to prevent pigmentation and 0.01% methylene blue.

For this study the following animal lines were used:

- AB: wild type line, obtained from the Wilson lab, University College London, London, United Kingdom.
- tg(gata1:dsRed)^{sd2}/tg(flk1:EGFP)^{S843} (from the Santoro lab, Molecular Biotechnology Center, Università di Torino, Torino, Italy),

a double transgenic line in which dsRed is under control of promoter of *gata1* gene, whereas GFP is under control of promoter of *flk1* gene [46].

Figure 14 Aquarium for fish breeding and mating.

3.2 RT-PCR analysis

RNA extraction and retrotranscription

Total RNAs were prepared from zebrafish oocytes and embryos at different developmental stages, using the RNAgents Total RNA Isolation System (Promega, Madison, WI), treated with DNaseI RNase free (Roche, Basel, Switzerland), to avoid possible contamination from genomic DNA, and then reverse transcribed using the ImProm-II Reverse Transcription System (Promega) and Random primers according to manufacturers' instructions. Primers specific for β–actin were used to check cDNA quality and possible genomic contamination.

PCR amplification

The cDNAs were then subjected to PCR amplification using GOTaq polymerase (Promega) for both pattern expression analysis and full-length sequence cloning. PCR products were separated by electrophoresis on a 1% agarose gel and stained with ethidium bromide. Primers are listed in Table 1.

Name	Sequence	Amplicon length
Expression analysis and probes production		
tm9sf4.Fprobe	5'-CTGCACAGCAACTCTTTACCC-3'	1002 bp
tm9sf4.Rprobe	5'-ATGAGACCCAGCCCAAAAAT-5'	
Full-length sequence cloning		
tm9sf4.F	5'-ATGACACGTGTATTCAAGATGG-3'	2279 bp
tm9sf4.R	5'-TTCAAAAGCATGAGACCCAG-3'	
Exon-skipping validation		
tm9I3E4.F	5´-CGTGTATTCAAGATGGCGGC-3´	604/435 bp
tm9I3E4.R	5´-CCTCTGCGTCCTCCAACTTT-3´	

Table 1 List of primers used for RT-PCR

3.3 Cloning and sequencing

PCR products were cloned into the pGEM-T easy Vector (Promega) and the plasmids were used to transform chemically competent cells DH5α^{TM} cells (Invitrogen) according to standard protocols. Plasmid DNA, after column purification with Wizard® Plus SV Midipreps DNA Purification

System (PROMEGA), was analyzed by electrophoresis on a 1% agarose gel and then the insert was controlled by Sanger sequencing.

3.4 Probes preparation

Template cloning

A 1002 bp cDNA template was generated by RT-PCR on total RNA extracted from 5 dpf (days post fertilization) embryos and primers listed in Table 1, as described before (Paragraph 3.3).

Plasmid digestion

The cDNA-containing plasmid was linearized with PstI restriction endonuclease and transcribed with T7 RNA polymerase (Roche) for the sense riboprobe synthesis or linearized with ApaI and transcribed with SP6 RNA polymerase (Roche) to synthesize the antisense probe.
The enzymatic digestions were performed using the following mix (100 μl):

- 10 μg plasmidic DNA in water solution
- Restriction endonuclease (3 U enzyme/μg DNA)
- Buffer 10X
- BSA 10X
- Nuclease-free H_2O

The reaction mix were incubated for at least 2 hours at 37 °C and the digestion were assessed by electrophoresis on 1% agarose gel. The DNA was extracted with 1 volume of phenol and following centrifugation the aqueous phase was collected and added with 10^{-1} volumes of sodium acetate and 2.5 volumes of ethanol. The mixture was incubated overnight at -20 °C, to precipitate DNA. After centrifugation, the pellet was washed with 70% ethanol and resuspended in nuclease-free H_2O.

Probe transcription

Probes were synthetized using MAXIscriptTM kit (Life Technologies) and dygoxigenin-UTP, according to manufacturers' instructions. The reaction mix was then treated with DNase at 37 °C for 15 minutes. The probes were purified using Sigma Spin^{TM} sequencing Reaction Clean-Up columns (Sigma) and analyzed by electrophoresis on 1% agarose gel, to determine the concentration.

3.5 Whole-mount in situ hybridization (WISH)

Embryos fixing

Embryos at the desired stage, after mechanical removal of chorion, were fixed with a solution of 4% PFA in PBS for 1 hour at room temperature, dehydrated with a graded methanol series in PBS and stored in 100% methanol at -20 °C.

Hybridization procedure

Whole-mount *in situ* hybridization (WISH) was performed as described by Thisse C. and colleagues [47] using 60% formamide, a hybridization temperature of 65 °C and 300 ng of probe per sample.

First day:

Embryos were rehydrated with a decreasing methanol series in PBS and they were washed four times in PBT (PBS 1X/1% Tween 20).

Successively, they were treated with a solution of 10 μg/ml proteinase K in PBT for different times, depending on the developmental stage.

The solution was removed and the reaction was blocked by incubation in PFA for 20 minutes at room temperature.

The embryos were washed 5 times with PBT and incubated in hybridization mix (HM) for 2-5 hours at 65 °C.

Successively, they were incubated overnight at 65 °C in HM, previously added with the probe.

Second day:

The following washes were performed:

- HM wash, 65 °C
- 75% HM wash/25% SSC 2X (15 minutes, 65 °C)
- 50% HM wash/50% SSC 2X (15 minutes, 65 °C)
- 25% HM wash/75% SSC 2X (15 minutes, 65 °C)
- SSC 2X (15 minutes, 65 °C)
- SSC 0.1X (30 minutes, 65 °C, X2)
- 75% SSC 0.1X/25% PBT (10 minutes, RT)
- 50% SSC 0.1X/50% PBT (10 minutes, RT)
- 25% SSC 0.1X/75% PBT (10 minutes, RT)
- PBT (10 minutes, RT)

The embryos were incubated in a PBT solution containing 2% sheep serum and 2 mg/ml BSA, for at least 2 hours at room temperature. Then, they were incubated in the same solution, previously added with anti-DIG antibody (1:5000), overnight at 4 °C.

Third day:

After antibody removal, embryos were washed 6 times with PBT at room temperature for 15 minutes and, then, 3 times with staining buffer for 5 minutes at room temperature.

The embryos were incubated in staining buffer added with 2.3 μl/ml NBT and 3.5 μl/ml BCIP.

To stop the staining, the buffer was removed and the embryos were washed in PBT.

Finally, a post-fixing was carried out by incubation in 1% PFA at room temperature for 30 minutes.
The embryos were washed with PBS and stored at 4 °C in PBS.

Solutions

10X PBS buffer: 180 g NaCl; 2 g KCl; 14.4 g Na_2HPO_4; 2.4 g KH_2PO_4, in milliQ H_2O (1 l final volume).

PBT buffer: 1% Tween 20 in 1X PBS

20X SSC pH 7 (Saline Sodium Citrate Buffer): 300 mM trisodium citrate; 3 M sodium citrate pH 7.0.

HM wash: 60% formamide; 5X SSC; 1M citric acid pH 6; 0.1% Tween 20; milliQ H_2O.

Hybridation mix (HM): HM wash; 500 μg/ml Yeast RNA; 50 μg/ml eparin.

Staining buffer: 100 mM NaCl; 100 mM Tris HCl pH 9.5; 50 mM $MgCl_2$; 0.1% Tween 20, milliQ H_2O.

Imaging

The embryos were transitioned to 87% glycerol/13% PBS 1X, by performing washes with a graded series of glycerol (30%, 50%, 75%). Images of stained embryos were taken with a Leica MZFLIII epifluorescence stereomicroscope equipped with a DFC 480 digital camera and IM50 Leica imaging software (Leica, Germany).

3.6 Histological sections

After hybridization the embryos were transitioned to PBS and dehydrated in a graded ethanol series (35%, 50%, 70%, 90%, 95%, and 100%),

transitioned to xylene and then embedded in paraffin wax (paraplast plus, Bio Optica).

Wax embedding and sectioning

After 2 washes with xylene (1 hour, RT), the embryos were incubated in 50% xylene/50% paraffin overnight at room temperature.
Three washes with liquid paraffin were performed (1 hour, 61 °C).
The embryos were positioned and properly oriented in inclusion molders that were filled with liquid paraffin. The blocks were allowed to cool at room temperature overnight.
Samples were then serially sectioned at 8 µm on a microtome (Leitz 1516). The sections were putted on slides (superfrost, Bio Optica) and dried at 37 °C.

Eosin staining and imaging

The wax was removed by consecutive washes in xylene.
The sections were rehydrated in a decreasing ethanol series (100%, 95%, 90%, 70%, and 50%), washed with dH_2O and stained with a water solution of eosin for 50 seconds.
After washing with dH_2O, the sections were dehydrated in a graded ethanol series and transitioned to xylene.
The slides were mounted with Eukitt (Bio Optica). All sections were observed at microscope Olympus BH-2 equipped with a Leica DCF480 digital camera and the software IM50.

3.7 Loss-of-function analysis

Wild type embryos, belonging to line AB, and double transgenic embryos, belonging to line tg(gata1:dsRed)^{sd2}/tg(flk1:EGFP)^{S843}, were injected with

antisense morpholino oligonucleotides. We designed an antisense translation blocking morpholino oligonucleotide (tm9sf4-MO), targeted to the start codon AUG, and a splicing morpholino oligonucleotide (tm9I3E4-MO), targeted to the junction between intron 3 and exon 4. Tm9sf4-MO was co-injected with an oligonucleotide targeted to *p53* (p53-MO), to suppress eventual off-target effects [48]. As a negative control, we injected a standard control morfolino (std-MO), targeted to human β-globin gene and having no targets in zebrafish. Morpholino oligonucleotides were synthesized by Gene Tools LLC (Oregon, USA). Morpholino sequences are reported in Table 2.

Morpholinos were dissolved in nuclease-free water at 1 mM concentration and stored at –80°C. Before injection they were dissolved in Danieau's solution (58 mM NaCl; 0.7 mM KCl; 0.4 mM $MgSO_4*H_2O$; 0.6 mM $Ca(NO_3)_2$; 5 mM Hepes pH 7.2) at the desired concentration. Rodamin dextran (Molecular Probes) was usually co-injected as a tracer. Therefore, the needle was filled with 5 μl of the following solution:

- Morpholino (at the desired concentration)
- Rodamin dextran (0.5 μl)
- Danieau's solution

Morpholino	**Sequence**
tm9sf4-MO	5'-TCACAGGAAGGATGTCAATGCGTCA-3'
tm9I3E4-MO	5'-CTCACCTGGAAACATATCAGCACCA-3'
std ctrl-MO	5'-CCTCTTACCTCAGTTACAATTTATA-3'
p53-MO	5'-GCGCCATTGCTTTGCAAGAATTG-3'

Table 2 Morpholino oligonucleotide sequences

Successively, 5 nl per embryo of this solution were microinjected at the 1–4 cells stage.

Fertilized eggs were collected in Petri dishes containing fish water and aligned on the edge of a slide placed in a dish (about 50 embryos/slide). The microinjections were performed using the "Micromanipulator 5171" (Eppendorf) and the microinjector "Cell Tram Oil" (Eppendorf) (Figure 15).

Figure 15 Microinjection system

After injection, embryos were raised in fish water at 28 ºC and observed up to the stage of interest. Before the phenotypic analysis, rodamin dextran positive embryos were selected and the chorion was mechanically removed. Injected embryos after 24 hpf were treated with PTU 1X (1-Phenil-2-thiourea, SIGMA; stock PTU 10X: 0.015 g of PTU powder in 50 ml of fish water) to inhibit pigment formation. The injected embryos were anaesthetized using tricaine 1X (Ethyl 3-aminobenzoate methanesulfonate salt, SIGMA; stock tricaine 25X: 0.08 g in 20 ml of distilled H_2O) in fish water and PTU 1X, to allow a better visualization and imaging. Images

were acquired by using a Leica MZ FLIII equipped with a Leica DCF480 digital camera and the software IM50.

3.8 Real time PCR analysis

RNA extraction and DNase treatment

Total RNAs were prepared from morphants at the desired developmental stage, using the RNAgents Total RNA Isolation System (Promega, Madison, WI). RNA was analyzed with Nanodrop, to measure the concentration.

1 μg of total RNA for each sample was treated with 1 Unit of DNaseI enzyme (cat. 18068-015, Invitrogen) at 25 °C for 15 minutes in a total volume of 10 μl. The enzyme was then inactivated adding 1 μl of ETDA (25 μM) and heating the reaction at 65 °C for 10 minutes.

Retrotranscription

cDNA was produced using 9 μl of the DNase with High-Capacity cDNA Reverse Transcription Kit (cat.4368814, Life Technologies) in a total volume of 20 μl, following manufacturers' instruction. The samples were incubated at 25 °C for 10 minutes (annealing), 37 °C for 120 minutes (reverse transcription) and, finally, at 85 °C for 5 minutes (inactivation).

Real Time PCR

qRT-PCR was performed with 7500 Real-Time PCR System (Life Technologies) using primers listed in Table 3 at the final concentration of 300 nM each, with SYBR Select Master Mix (cat. 4472920, Life Technologies), following manufacturers' instructions. Each single reaction was performed with a cDNA amount corresponding to 5 ng of original total RNA. All the analysis were performed by calculating relative quantification

with the ΔΔCt approach, using *Rpl8* as endogenous control and calculating the standard error among triplicate reactions.

Primer	Type	Sequence
ZF_Fgf8_F	Forward	5'-GAGTTATCTATTCCTTCACCTCTTTGC-3'
ZF_Fgf8_R	Reverse	5'-TCACTCACATGCTGTGTAAAATTAGG-3'
ZF_SHHa_F	Forward	5'-CCAAAGCCCACATTCATTGC-3'
ZF_SHHa_R	Reverse	5'-AAACAGCCCCCAGATTTCG-3'
ZF_Rpl8_F	Forward	5'-CCGTTGTTGGTGTTGTTGCT-3'
ZF_Rpl8_R	Reverse	5'-TTGGCCTTGTATTTGTGGTAAGC-3'
ZF_Wnt1_F	Forward	5'-CCCACAGCCCCAATGTCTT-3'
ZF_Wnt1_R	Reverse	5'-CACCAGCACTTGTAATGGCAAA-3'
ZF_Egr2a_F	Forward	5'-AAGGAGGCACACAAAAATCCA-3'
ZF_Egr2a_R	Reverse	5'-TGTGAGGGCCCACAGAAAG-3'
ZF_OTX2_F	Forward	5'-ACCCAGCGACTCCTCGAAA-3'
ZF_OTX2_R	Reverse	5'-GCACATCTAGTTGCGCTCTAGTAAA-3'
ZF_OTX1a_F	Forward	5'-TATCCCACGAATCCTCGTAAACA-3'
ZF_OTX1a_R	Reverse	5'-CTCTCCAAGATGTCCAGCTGAGT-3'
ZF_CDH1_F	Forward	5´-TGTAGCGAGTCAAATGGCTTGT-3´
ZF_CDH1_R	Reverse	5´-CCACTCGAAAAGACCTGAAAAAGA-3´
TWIST2_F	Forward	5'-AGGGCGCGTGGTCGAT-3'
TWIST2_R	Reverse	5'- AGTAAACAGTCCGTTCGGCATT-3'

Primer	Type	Sequence
TWIST1a_F	Forward	5'-CCATGTCAACATCCCACTAACG-3'
TWIST1a_R	reverse	5'-CCATGTCAACATCCCACTAACG-3'
TWIST1b_F	Forward	5'-GGGCGCTTGGTCCATGT-3'
TWIST1b_R	Reverse	5'-GCTCACGGTTTGACCATTTAAAA-3'
ZEB2a_F	Forward	5'-CAGCCACCTTTGCTGAGAT-3'
ZEB2a_R	Reverse	5'-ATCCCCCTGGAAGCCTTGT-3'
ZEB2b_F	Forward	5'-GGTACAGATGAACTGAAGGCTGATT-3'
ZEB2b_R	Reverse	5'-ACTTTCAGTGTCCACCAGTTTACG-3'

Table 3 List of primers used for qRT-PCR

4. RESULTS

4.1 *Tm9sf4* expression analysis

4.1.1 Tm9sf4 expression during embryonic development

Zebrafish *tm9sf4* full-length transcript was amplified by RT-PCR, using cDNA from 5 dpf embryos and, after cloning, the absence of mutations or rearrangements was evaluated by sequencing (NM_200510).

To determine the expression of *tm9sf4* gene throughout the zebrafish embryonic development, we performed RT-PCR analyses using total RNAs prepared from oocytes and embryos at different developmental stages. The *tm9sf4* transcript was detected in all of the analyzed stages, from oocytes to 5 dpf (Figure 16), suggesting that the expression is both maternal and zygotic. These results are consistent with the previous findings [26].

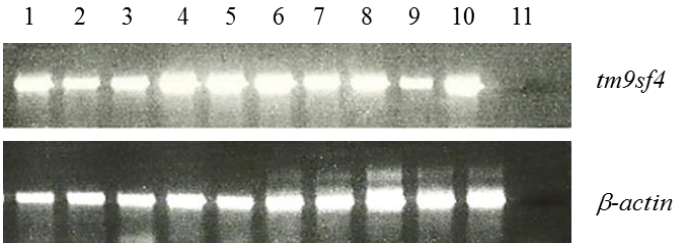

Figure 16 RT-PCR expression pattern of the zebrafish *tm9sf4* gene during embryonic development. (1) oocytes; (2) 64-cells; (3) 30% epiboly; (4) 50% epiboly; (5) tail bud; (6) 5-8 somites; (7) 15-20 somites; (8) 26 hpf; (9) 2 dpf; (10) 5 dpf; (11) negative control.

4.1.2 Tm9sf4 expression in embryonic tissues

In order to investigate *tm9sf4* specific expression in embryonic tissues by whole mount *in situ* hybridization (WISH), first we determined the hybridization conditions and tested prepared probes, carrying out trials with embryos at 24 hours post fertilization (hpf).

Successively, the analysis was performed, using selected conditions, on embryos at different developmental stages: 10 somites, 15 somites (not shown), 24 hpf (Figure 17, A-C), 48 hpf (Figure 17, D-F) and 72 hpf (Figure 17, G-I).

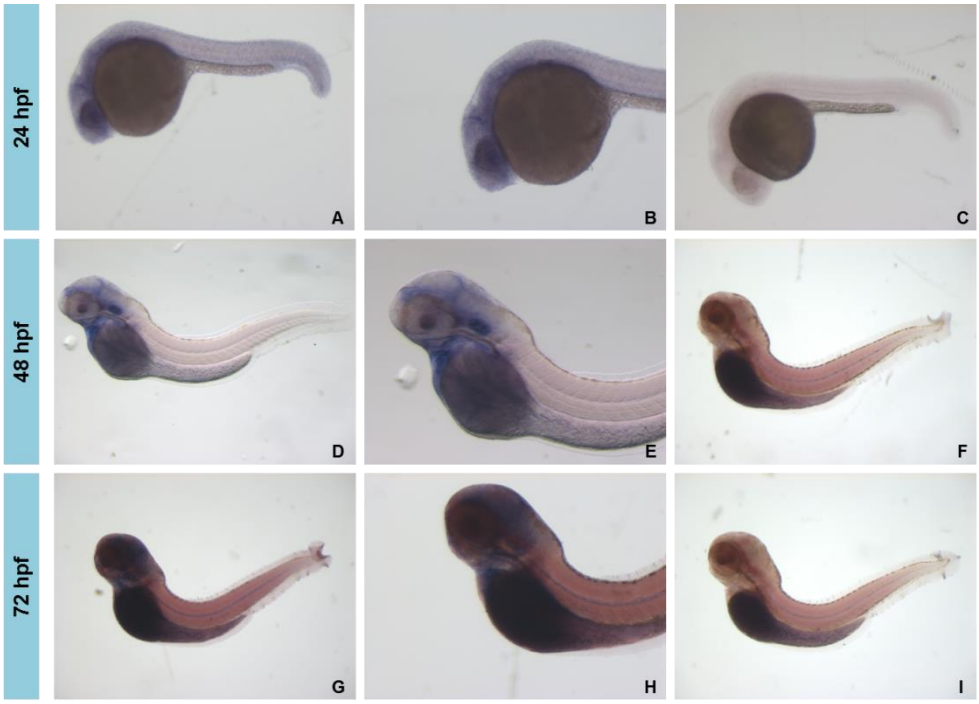

Figure 17 Expression panel of embryos at different developmental stages, obtained by whole mount *in situ* hybridization, using an antisense probe, targeting the *tm9sf4* transcript. Negative controls were performed by hybridization with the sense probe. (A) *tm9sf4* expression at 24 hpf (magnification 8X), (B) head detail (magnification 10X) and (C) negative control (magnification 8X). (D) *tm9sf4* expression in 48 hpf embryos (magnification 6.3X), (E) head detail (magnification 10X) and (F) negative control (magnification 6.3X). (G) *tm9sf4* expression in 72 hpf embryos (magnification 6.3X), (H) head detail (magnification 10X) and (I) negative control (magnification 6.3X).

The results suggested that the gene is mainly expressed in the central nervous system (CNS) in all the analyzed stages: in particular, the expression was detected in the telencephalon, mesencephalon and cerebellum, and a marked expression was detected at the eye level, both in

the retina and crystalline lens. Moreover, in 24 hpf embryos a superficial signal in the tail was present (Figure 17, A), while 72 hpf embryos showed a signal in notochord (Figure 17, G).

To better understand the specific localization of the embryonic signals, the stained embryos were wax embedded and histological sections were obtained as described in materials and methods.

At 24 hpf the sections of the head showed a scattered signal in the brain and eye and a stronger signal in the crystalline lens and in the periventricular wall of the diencephalon and mesencephalon, both at the tegmentum and tectum level (Figure 18, B). Moreover, *tm9sf4* gene expression was detected in the periventricular wall of the hindbrain and in the otic vesicles (Figure 18, C). At the tail level, we detected a punctuated superficial signal in somites that may be either muscular or epithelial (Figure 18, D).

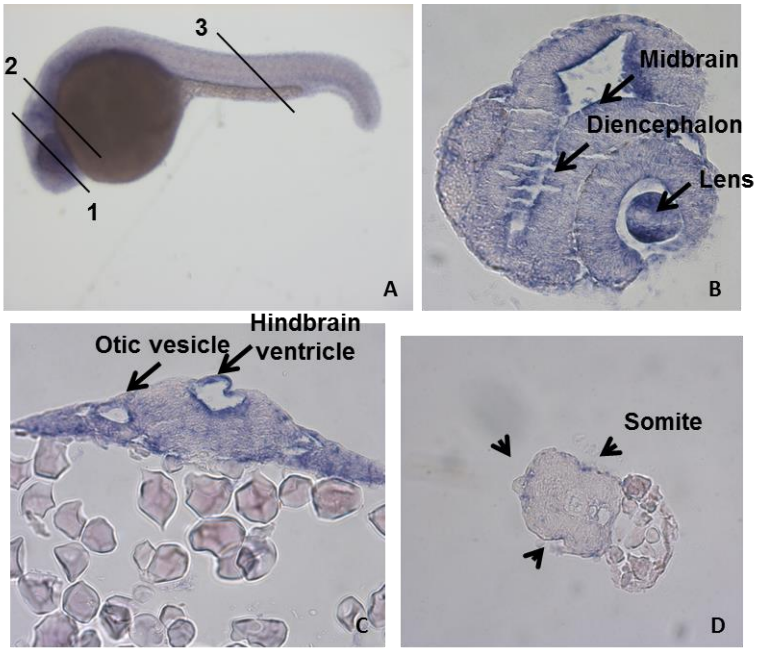

Figure 18 (A) *tm9sf4* expression in 24 hpf embryos, obtained by whole mount *in situ* hybridization (magnification 8X). (B-D) Histological sections (8 μm) of the

stained embryo in the regions indicated in A by the lines 1, 2 and 3 respectively (B-C, magnification 40X and D, magnification 20X).

At 48 hpf, embryos showed a strong expression signal in the stomodeum wall (Figure 19, B), in the periventricular wall of the diencephalon (Figure 19, C), in the internal wall of otic vesicles and in the myelencephalon (Figure19, D). We also detected a signal in the endodermic tissue of the gastrointestinal tract (Figure19, E) and in the pectoral fin buds (Figure19, F), while no expression was found in the tail (Figure 19, G).

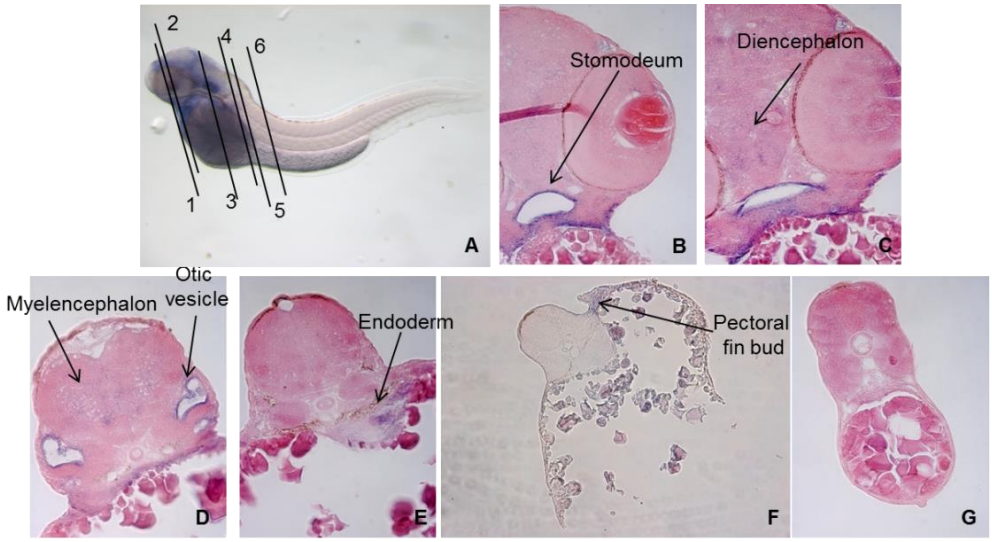

Figure 19 (A) *tm9sf4* expression in 48hpf embryos, obtained by whole mount *in situ* hybridization (magnification 6.3X). (B-G) Histological sections (8 μm) of the stained embryo at the levels indicated by lines 1-6 respectively (B, C, D, E, G, magnification 40X; F, magnification 20X).

Embryos at 72 hpf showed a stronger expression in the diencephalon, optic tectum (Figure 20, B), otic vesicles and pharynx (Figure 20, C). Finally, a marked signal was detected in the notochord (Figure 20, D).

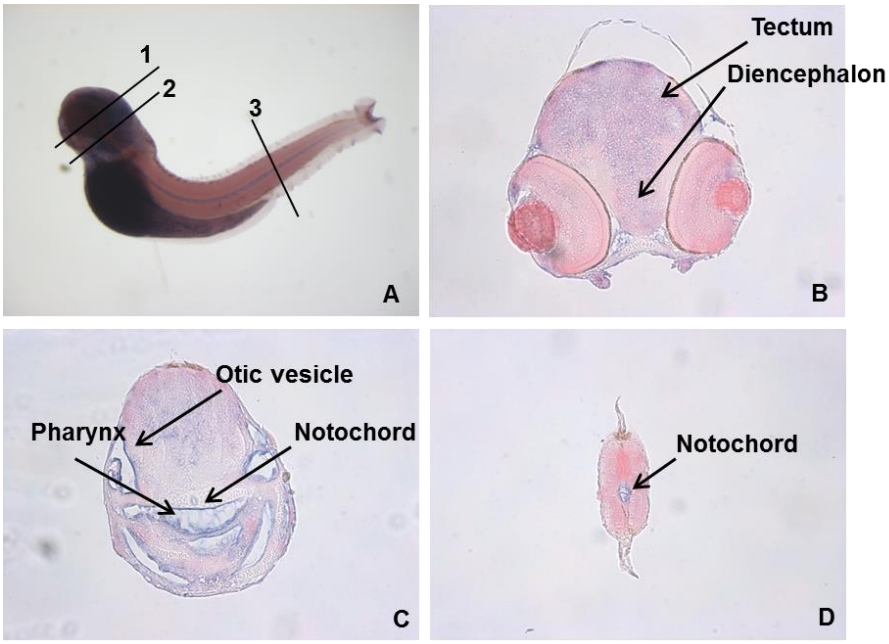

Figure 20 (A) *tm9sf4* expression in 72 hpf embryos, obtained by whole mount *in situ* hybridization (magnification 6.3X). (B-D) histological sections (8 μm) of the stained embryo at the levels indicated by lines 1, 2, 3 (magnification 20X).

4.2 Loss-of-function analysis

4.2.1 Injection of translation blocking morpholino oligos in AB line

In order to investigate the function of *Tm9sf4* protein *in vivo* during embryonic development, we performed loss of function experiments by injection of antisense morpholino oligonucleotides (MOs) in 1-4 cell stage embryos. We started this study using an AUG-targeted oligonucleotide (tm9sf4-MO), which acts as a translation-blocking morpholino. As a negative control we injected a standard control morpholino (std-MO), which targets the human β-globin gene and has no targets in zebrafish.

At first, we tested two different doses of tm9sf4-MO: 0.5 and 1 pmol/embryo. At 48 hpf the morphants showed a low survival rate (39%

and 22% of the total number of *tm9sf4* morphants, respectively). The surviving embryos displayed a marked necrosis in the central nervous system and severe morphological defects. Therefore, we decided to co-inject the tm9sf4-MO with an oligo targeting *p53* (p53-MO), in order to suppress possible off-target effects [48].

Then we performed the dose/survival curve by co-injecting different doses of the tm9sf4-MO and p53-MO at the molar ratio of 1:1.5. The embryos were visually followed for at least three days after injection. We took into account the survival rate at 48 hpf, because within this period the majority of the morphants died.

In concordance with the study of Nasevicius and Ekker [49], we obtained a highly specific series of phenotypes dependent on dose. The results are summarized in table 4 and the plots reported in figure 21; the corresponding phenotypes are shown in figure 22.

As expected, the higher the dose of injection, the lower was the survival rate. Moreover, for all the doses tested, the survival rate was higher in *tm9sf4/p53* morphants than in *tm9sf4* morphants and lower in morphants than in control embryos. These results suggest that the severe phenotypes, observed following the injection with the *tm9sf4* morpholino alone, were partially due to off-target effects mediated by *p53* activation. This effect leads to the activation of the *p53*-dependent cell death pathway, in which a N-terminal truncated *p53* isoform is transcribed from a recently recognized internal promoter [48].

Additionally, based on these data, we established that the optimal dose of the tm9sf4-MO was 0.6 pmol/embryo, which allowed a survival rate of 79% in double morphants and induced detectable defects in surviving embryos.

	Survival rate (%)		
Dose of tm9sf4-MO (pmol/embryo)	tm9sf4-MO	tm9sf4-MO/ p53-MO	std-MO
0.5	65 (n=31)	81 (n=34)	84 (n=25)
0.6	56 (n=36)	79 (n=29)	93 (n=41)
0.8	10 (n=40)	14 (n=42)	77 (n=39)
1	7 (n=37)	12 (n=33)	81 (n=42)

Table 4 Dependence of the embryonic survival rate on the dose of tm9sf4-MO injected in 1-4 cells embryos.

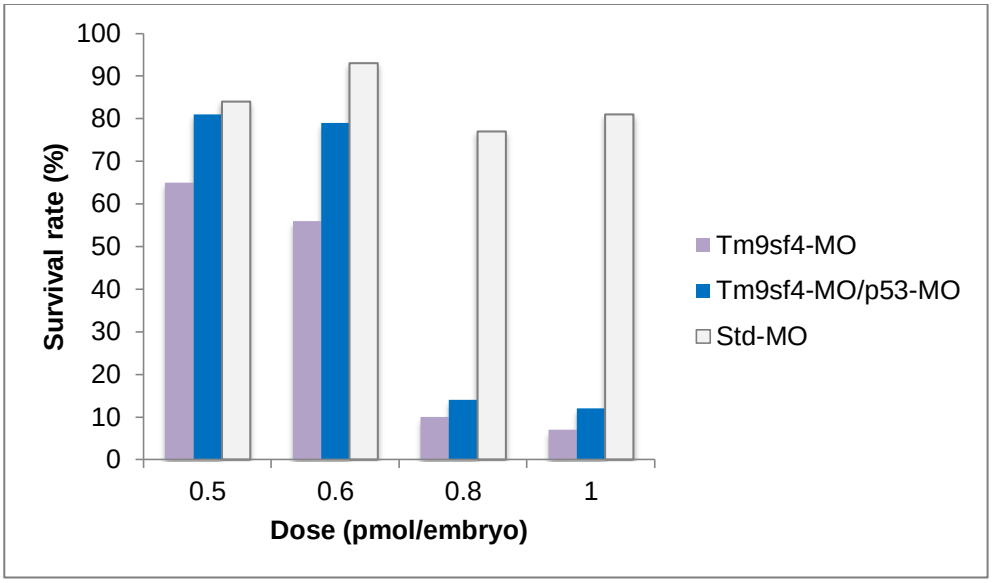

Figure 21 Tm9sf4-MO and tm9sf4-MO/p53-MO dose/survival assay.

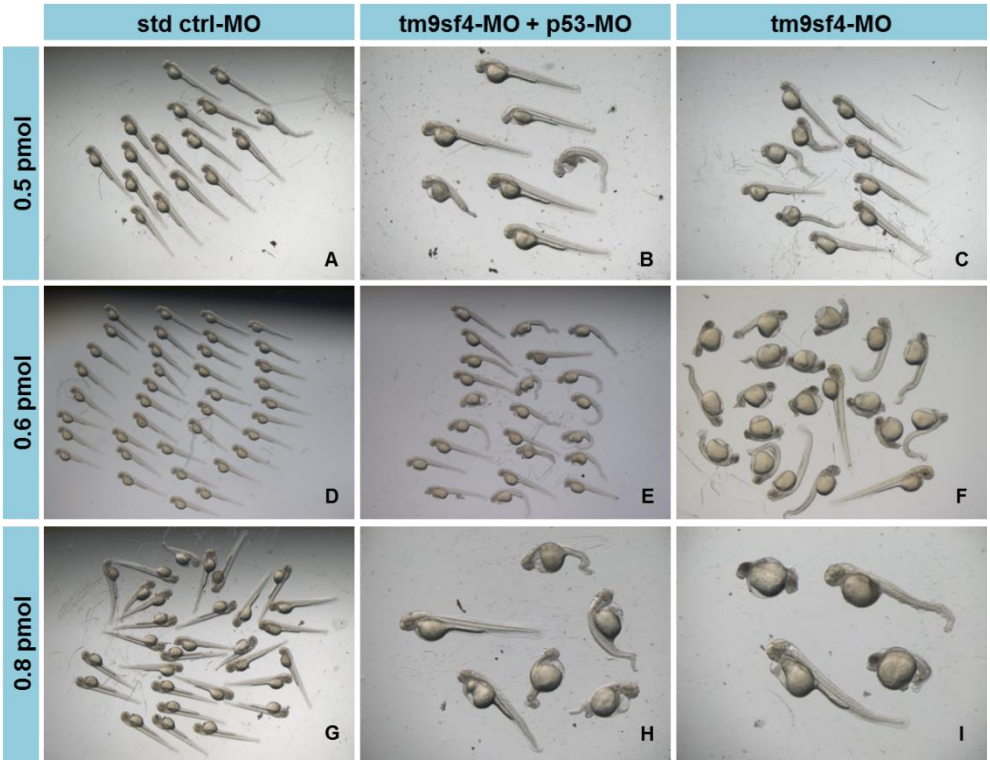

Figure 22 Effects of Tm9sf4 protein loss-of-function on embryos at 48 hpf, following injection with different doses of the tm9sf4-MO (C, F and I), Tm9sf4/p53-MO at the ratio 1:1.5 (B, E and H) and std-MO (A, D, G). Panels in lines 1, 2 and 3 correspond to 0.5 pmol, 0.6 pmol and 0.8 pmol of morpholino, respectively (C: magnification 1.25X; B and F: magnification 1.6X; A, G, E and D: magnification 1X; I: magnification 2.5X; H: magnification 2X).

At the selected dose we obtained three phenotypic classes, one having a phenotype similar to wild type embryos (43% of total number of morphants; Figure 23, A), one having mild phenotype (35%; Figure 23, B) and one having severe phenotype (22%; Figure 23, C).

At 24 hpf, *tm9sf4/p53* morphants displayed necrosis in the head, even if it was markedly reduced with respect to *tm9sf4* morphants, and they showed a consistent tail bending. Furthermore, like in *tm9sf4* morphants, the brain compartmentation was not as well defined as in control embryos (Figure 24, A-C).

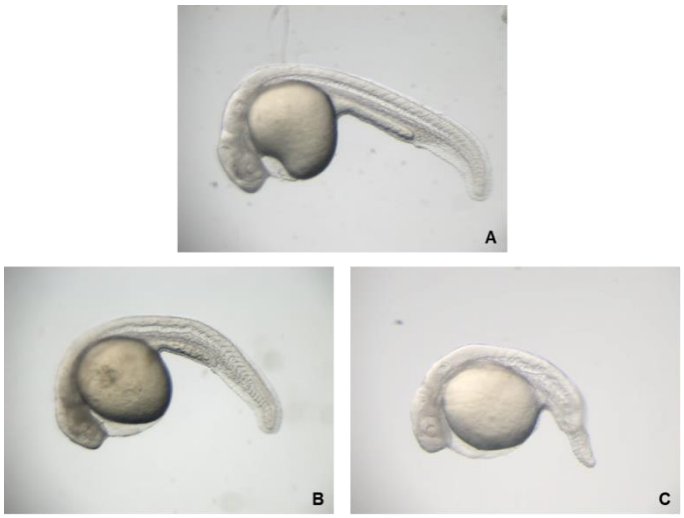

Figure 23 Phenotypic classes obtained by injection of 0.6 pmol/embryo of tm9sf4-MO (24 hpf embryos, n=53): (A) WT-like; (B) Mild; (C) Severe.

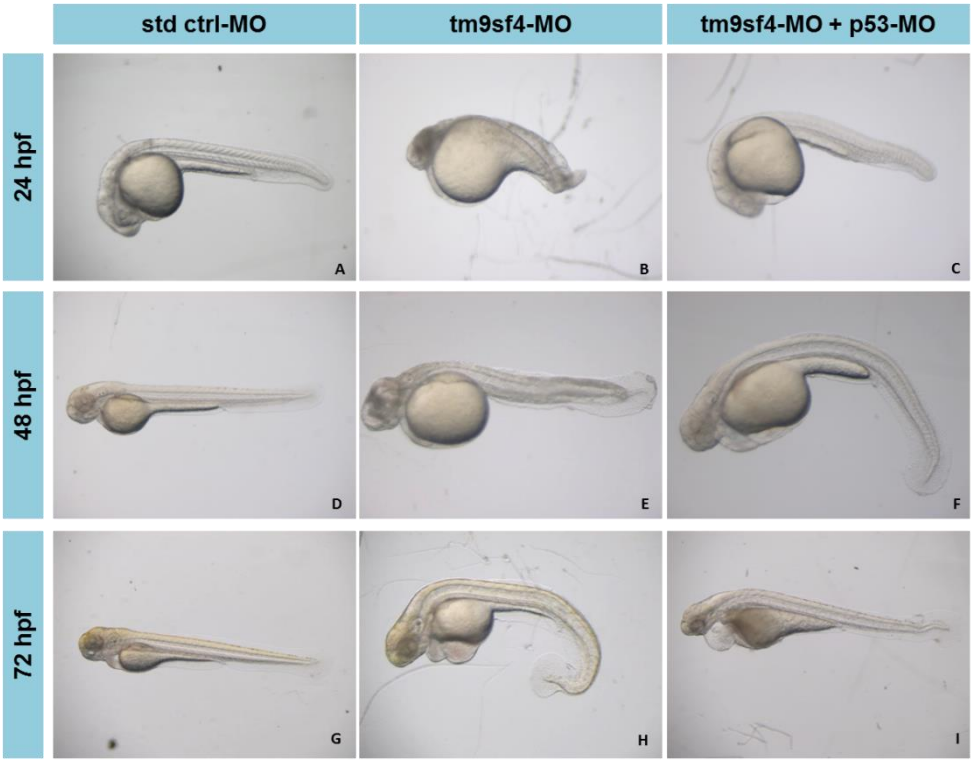

Figure 24 Effects of Tm9sf4 protein loss-of-function on embryos at 48 hpf, following injection with different doses of tm9sf4-MO (C, F, I), Tm9sf4/p53-MO at

the ratio 1:1.5 (B, E, H) and std-MO (A, D, G). The first line corresponds to 0.5 pmol, the second to 0.6 pmol and the third to 0.8 pmol of morpholino (C: magnification 1.25X; B and F: magnification 1.6X; A, G, E, D: magnification 1X; I: magnification 2.5X; H: magnification 2X).

At 48 hpf (Figure 24, D-F) this defect was partially restored and the necrosis was reduced. The embryos displayed also cardiac edema and some problems in blood flow; the circulation was either not complete or totally absent in the tail. The same defects persisted at 72 hpf (Figure 24, G-I).

4.2.2 Injection of splicing morpholino in AB line

We designed a splicing morpholino (Tm9i3e4-MO) targeting the junction between intron 3 and exon 4, which was expected to induce the skipping of exon 4 (164 bp), during mRNA splicing.

Morpholino activity was validated by RT-PCR on cDNA prepared from 24 hpf embryos, following injection with tm9I3E4-MO, using specific primers, listed in materials and methods (Table 1). The results confirmed that tm9I3E4-MO was able to induce exon skipping (Figure. 25).

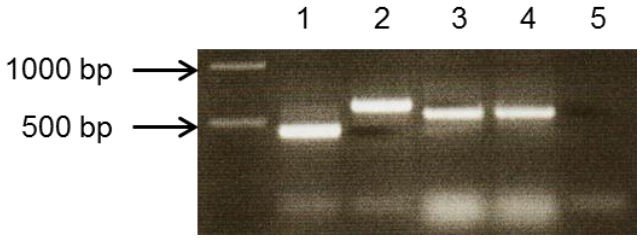

Figure 25 Splicing morfolino validation, carried out by RT-PCR on 24 hpf embryos injected with tm9I3E4-MO (1) and std-MO (2); β-actin PCR on 24 hpf embryos injected with tm9I3E4-MO (3) and std-MO (4); negative control (5).

A dose/survival curve was performed, by injecting different doses of tm9I3E4-MO. Also in this case the survival rate was inversely proportional to the morpholino dose (Table 5, Figure 26) and dose-dependent phenotypes were observed (Figure 27).

Dose (pmol/embryo)	Survival rate (%)	
	tm9I3E4-MO	std-MO
0.5	92 (n=52)	95 (n=41)
0.7	81 (n=36)	96 (n=25)
0.8	79 (n=29)	84 (n=25)
1	50 (n=58)	91 (n=45)

Table 5 Dependence of the embryonic survival rate on the dose of Tm9I3E4-MO injected.

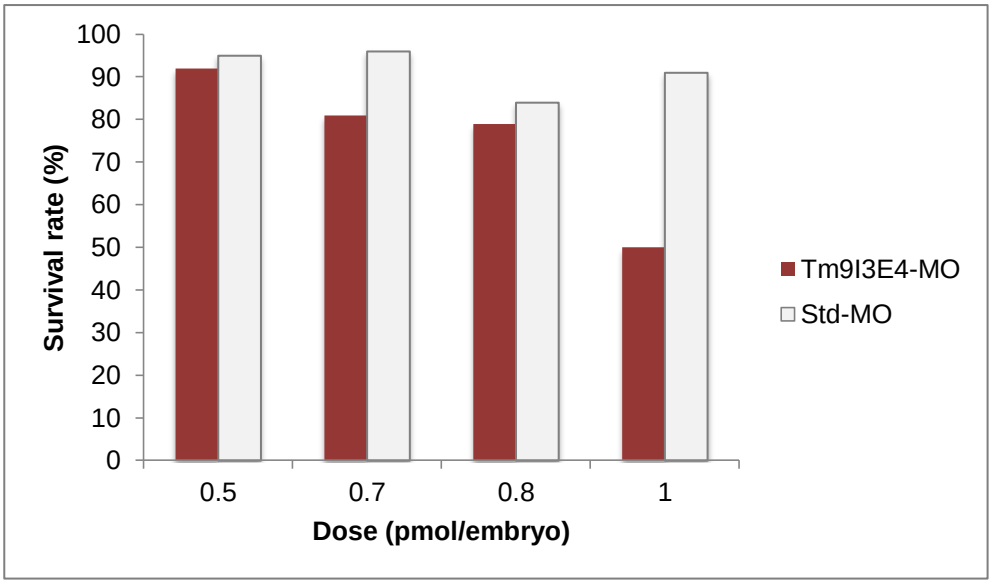

Figure 26 Tm9I3E4-MO dose/survival assay.

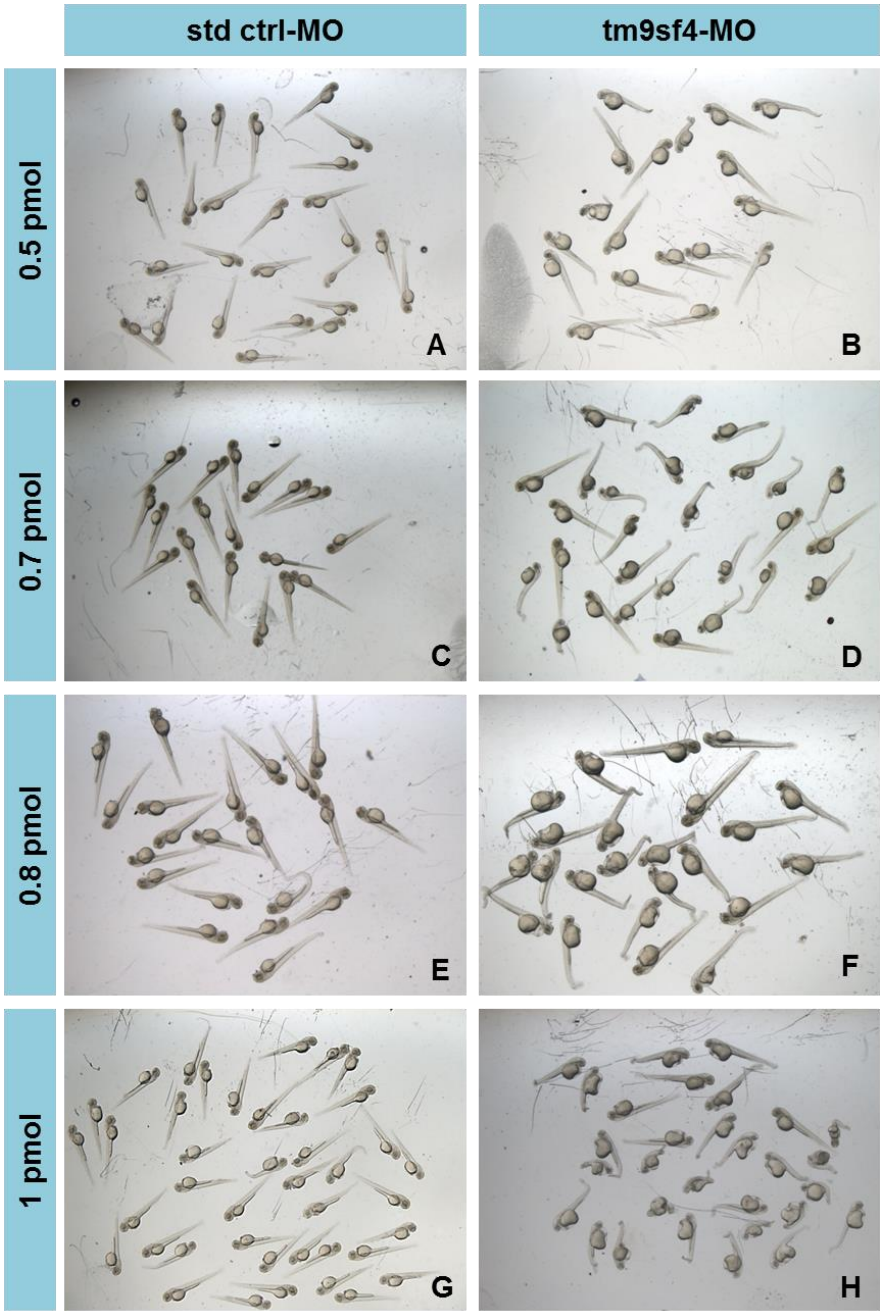

Figure 27 Effects of Tm9sf4 protein loss-of-function on embryos at 48 hpf, following injection with different doses of std-MO (A, C, E, G, magnification 0.8X) and Tm9I3E4-MO (B, D, H, magnification 1X;F, magnification 1.25X).

Based on these results, we established that the optimal dose of Tm9I3E4-MO was 0.8 pmol/embryo that allowed a survival rate of 79% in morphants. At this dose, three phenotypic classes were identified, based on tail bending, which was the most evident defect.

At 24 hpf, 4% of *Tm9I3E4* morphants were morphological similar to std-MO injected embryos (Figure 28, A), the *tm9I3E4* morphants displaying mild tail bending amounted to 69% (Figure 28, B), and the class showing a marked tail bending corresponded to 27% of the total number of morphants (Figure 28, C). In particular, we observed defects in the region of the intermediate cell mass (ICM), the site where primitive hematopoiesis and vessels development occur. In addition, we could detect a slight necrosis in the head. These phenotypes were consistent with previous results (Figures 23 and 24), even if the CNS was more strongly affected by tm9sf4-MO/p53-MO injection with respect to tm9I3E4-MO injection.

At 48 hpf, the three phenotypic classes corresponded to 13%, 26% and 61% of the total number of the surviving *tm9I3E4* morphants, respectively (Figure 28, D-F). The necrosis in the head was significantly reduced, while the defects in the tail persisted. In addition, in the vast majority of our morphants the circulation was either not complete or totally absent and some of them displayed cardiac edema or blood stasis in the tail, as in the case of tm9sf4-MO/p53-MO injection.

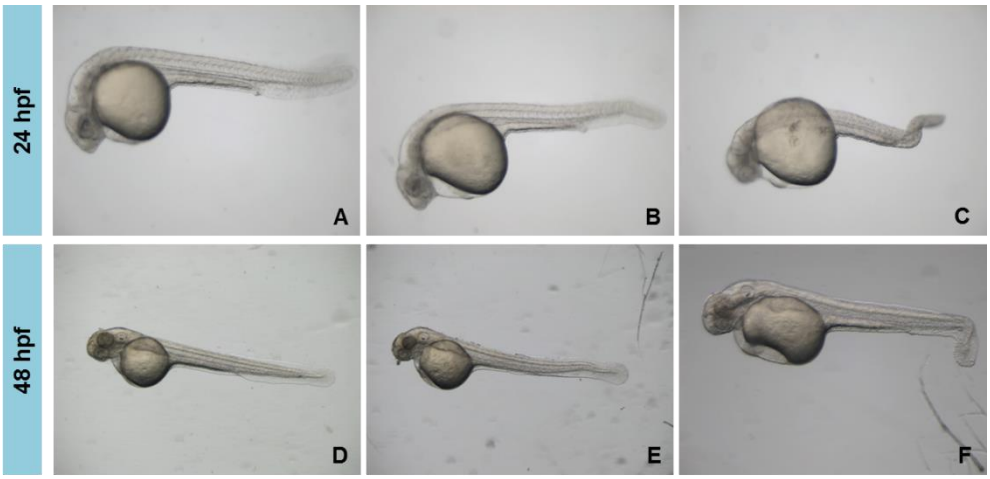

Figure 28 Phenotypic classes obtained by injection of 0.8 pmol/embryo of tm9I3E4-MO. (A-C) 24 hpf embryos (n=26); (D-F) 48 hpf embryos (n=23). A, B, C and F, magnification 6.3X; D and E, magnification 4 X.

4.3 The role of Tm9sf4 protein in the central nervous system

Since both the *tm9sf4/p53* and *tm9I3E4* morphants displayed defects in the central nervous system, we planned to study the expression of specific markers in the *tm9sf4* morphants compared to controls, to individuate the brain sub-structures that are affected by Tm9sf4 protein downregulation. We selected a set of genes that are representative markers of specific structures in the central nervous system (*fgf8*, *shha*, *wnt1*, *otx2*, *otx3 -otx1a-*, *krox20 -egr2a-*). The expression of *fgf8* (fibroblast growth factor 8), *shha* (*sonic hadgehog a*), *otx2* (*orthodenticlehomeobox 2*) and *wnt1* (Wingless-type MMTV integration site family member 1) was assayed by WISH on 24 hpf embryos (AB line), previously injected with tm9sf4-MO/p53-MO.

In situ hybridization for *fgf8* showed that in the *tm9sf4* morphants the signals were diffused and that the brain regions seemed to be less organized with respect to control embryos. The midbrain-hindbrain

boundary (MHB) appeared thicker than in controls and in general the marker was at least apparently upregulated in *tm9sf4* morphants (Figure 29, A-D).

Then we analyzed the expression of *shha that* marks the floor plate and notochord. In *tm9sf4* morphants the expression in the floor plate was similar to controls, whereas the notochord had an altered morphology respect to std-MO injected embryos (Figure 29, E-H).

Also *otx2* signal was more diffused in *tm9sf4/p53* morphants if compared to control embryos and the brain regions were not well defined (Figure 29, I-L).

Wnt1 expression confirmed that the MHB was thicker in *tm9sf4* morphants than in controls and also in this case the marker appeared upregulated in our morphants (Figure 29, M-P).

Furthermore, the expression level of all these markers was assessed by qRT-PCR on RNAs extracted from 24 hpf *tm9sf4/p53* morphants and compared to control embryos (Figure 30). According to WISH analyses, the results showed that *fgf8*, *shha*, *wnt1* and *otx3* (*otx1a*) were upregulated in morphants, following *tm9sf4* downregulation. In particular, *fgf8* was the most differentially expressed; according to *in situ* hybridization results. In contrast, the expression level of *otx2* and *krox20* (*egr2a*) was lower in tm9sf4/p53-MO injected embryos than in controls.

These results are consistent with the literature about the pathways involved in zebrafish brain development [50], [51], [52].

They were also confirmed by qRT-PCR on RNAs from 24 hpf *tm9l3E4* morphants, with the exception of *krox20*, which was significantly up-regulated in *tm9l3E4* morphants, while it was downregulated in *tm9sf4/p53* morphants, and *otx3*, which underwent a stronger upregulation in *tm9sf4/p53* morphants with respect to *tm9l3E4* morphants (Figure 31).

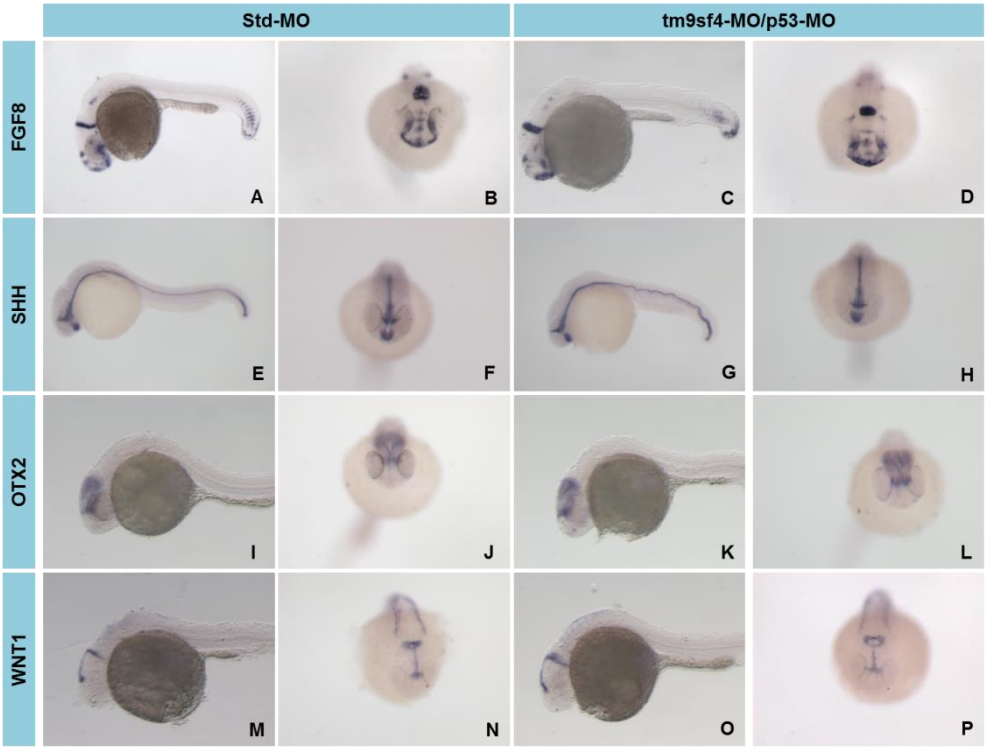

Figure 29 CNS marker expression in *tm9sf4/p53* morphants and in std-MO inhected embryos.

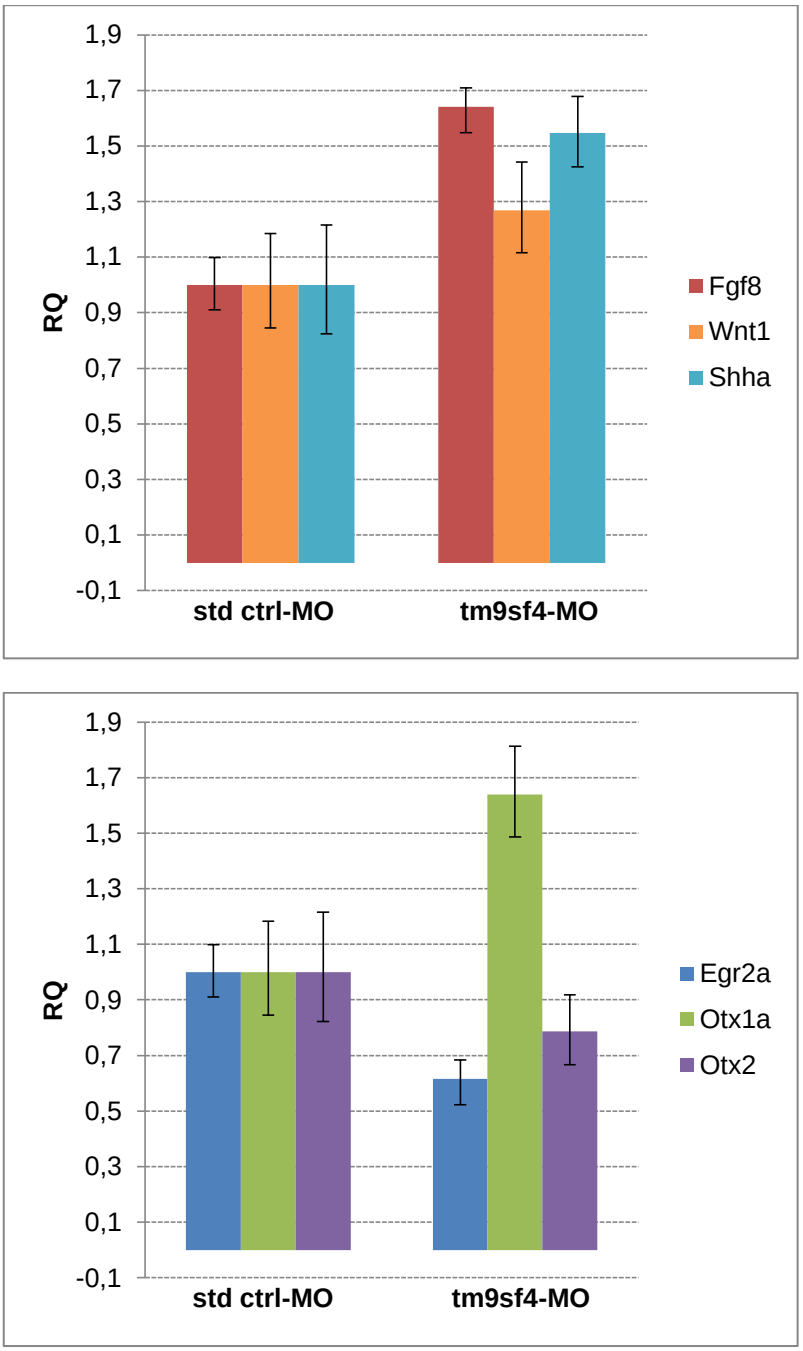

Figure 30 Expression level of specific CNS markers at 24 hpf following Tm9sf4 protein downregulation by injection of tm9sf4-MO/p53-MO. Vertical bars represent standard errors calculated among triplicate reactions.

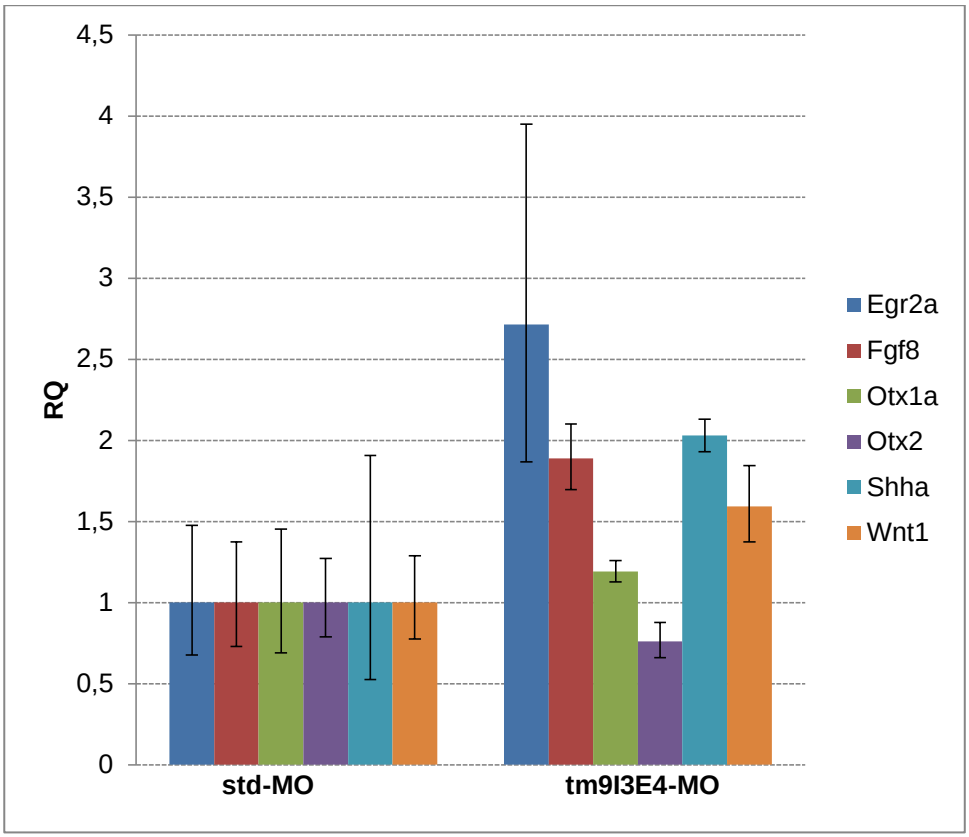

Figure 31 Expression level of specific CNS markers at 24 hpf following *tm9sf4* downregulation by injection of tm9I3E4-MO. Vertical bars represent standard errors calculated among triplicate reactions.

4.4 The role of Tm9sf4 protein in zebrafish blood system

Since Tm9sf4 protein downregulation caused circulation defects in the majority of embryos and, in some cases, cardiac edema and blood stasis in the tail, we wanted to further investigate this issue by performing loss-of-function studies, using a double transgenic line tg(gata1:dsRed)^{sd2}/tg(flk1:EGFP)^{S843}, in which blood vessel endothelium is labelled in green and circulating elements are labelled in red.

The embryos, previously injected with tm9I3E4-MO or std-MO (0.8 pmol/embryo), were observed at 48 hpf. The survival rate was 71% for *tm9I3E4* morphants and 89% for controls.

The morphants could be divided in three phenotypic classes, based on the tail bending. The first class, having a straight tail, corresponded to 23% of the total number of survived embryos (n=65). The majority of them (80%) displayed a complete or partial blood circulation at the tail level. The second class, showing a slight tail bending, amounted to 43% of the total number of morphants. In all the embryos belonging to this class the circulation was totally absent in the tail. Finally, the third class, composed by embryos with severe defects, corresponded to 34% of the total number of morphants and it included non-circulating embryos.

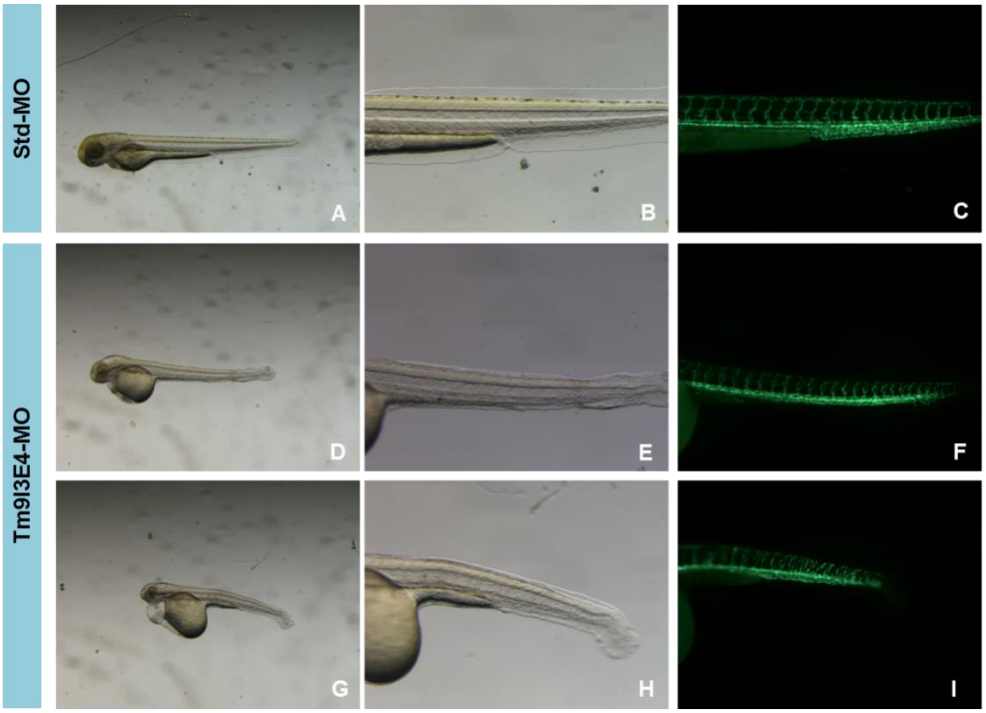

Figure 32 Loss-of-function analysis on double transgenic line tg(gata1:dsRed)^{sd2}/tg(flk1:EGFP)^{S843}, carried out by injecting 0.8 pmol/embryo of std-MO (A-C) or tm9I3E4-MO (D-I). (D-F) wild type-like phenotype; (G-I) mild

phenotype. The magnification is 32X for the whole embryos and 80X for the tail details.

For which concerns the first class of morphants, the main axial vessels (Dorsal Aorta and Posterior Cardinal Vein) and intersomitic vessels did not display detectable defects (Figure 32, D-F). Taking into account the second class, in which the circulation was absent, despite the tail did not have significant morphological defects, we observed that the embryos reported defects at the intersomitic vessels, which are formed by angiogenesis (Figure 32, G-I).

4.5 Expression analysis of EMT-associated markers

Our preliminary results suggested that *tm9sf4* is involved in the process of epithelial to mesenchymal transition (EMT) in LA7 cells, used as a model of mammary gland cancer stem cell (CSC). In fact, we demonstrated that the expression level of *tm9sf4* was higher in LA7 CSCs if compared to LA7 progeny (Figure 7). Moreover, *tm9sf4* downregulation induced changes in LA7 CSCs morphology, leading them to trans-differentiate to mesenchymal-like cells (Figure 8). In support of this, the expression level of EMT-associated markers (*twist1, zeb1, zeb2)* increased following *tm9sf4* downregulation (Figure 9). Since mechanisms and pathways involved in EMT are conserved in all vertebrates, we wanted to investigate *tm9sf4* role in this process, using zebrafish as a model system. First, we verified that these genes are conserved in *D. rerio* and that they have functions similar to mammals. In particular, in zebrafish we found two orthologues for mammals *twist1* (*twist1a* and *twist1b*), two for *zeb2* (*zeb2a* and *zeb2b*) and one for *twist2*. Then, we evaluated their expression level by qRT-PCR, performed on RNAs from embryos previously injected with tm9sf4-MO/p53-MO. In agreement with our previous results obtained with LA7 cells, *twist2*

and *zeb2* resulted upregulated in *tm9sf4/p53* morphants with respect to control embryos, at 24 hpf, a stage of zebrafish development associated with neurulation, while *twist1* expression was substantially not affected (Figure 33).

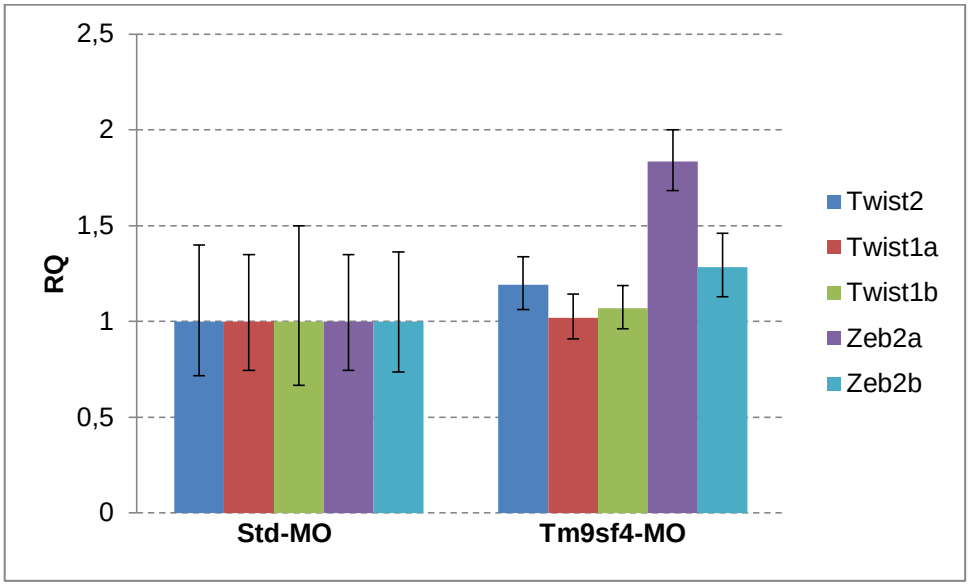

Figure 33 Expression levels of EMT markers in *tm9sf4/p53* morphants compared to control embryos (std-MO) at 24 hpf. Vertical bars represent standard errors calculated among triplicate reactions.

Successively, since gastrulation is the earliest stage in which the EMT occurs, we evaluated the expression level of the same markers in *tm9sf4/p53* morphants at 80% epiboly. *Tm9sf4* downregulation did not significantly affect the expression level of all EMT markers tested (not shown), with the exception of *zeb2a* and *zeb2b*, which are markedly reduced in morphants (Figure 34). This result is in contrast to that observed with *tm9sf4* downregulation at 24 hpf. Therefore, since *tm9sf4* downregulation did not result in the change of the EMT markers tested except for *zeb2*, it may not act on these markers in regulating EMT during gastrulation.

However, Tm9sf4 protein downregulation induced a decrease of the E-cadherin (*cdh1*) expression (Figure 34).

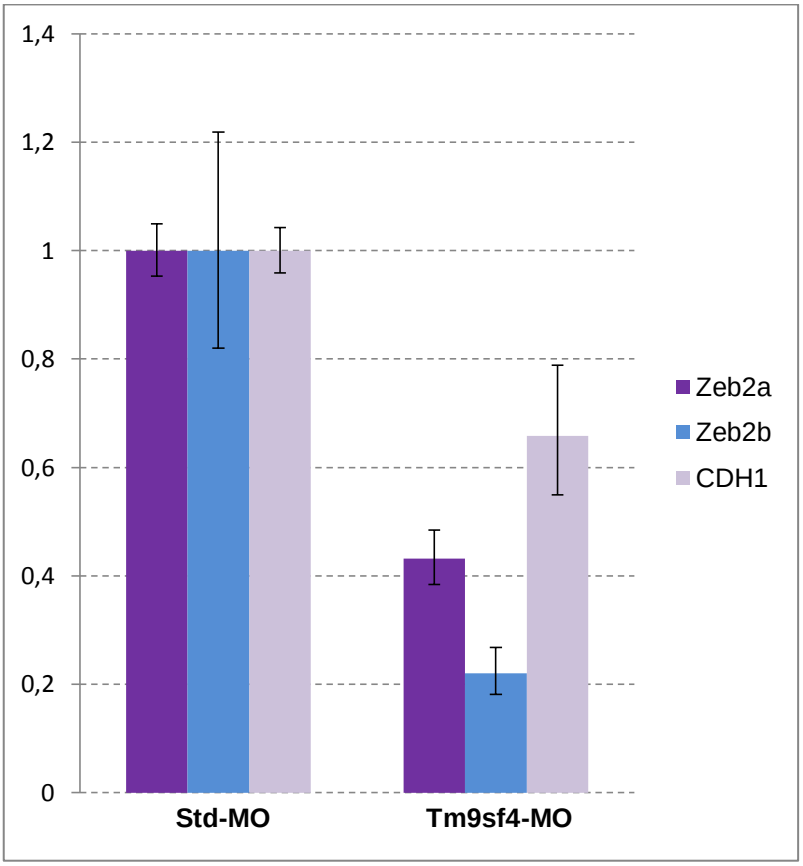

Figure 34 Expression levels of EMT markers in *tm9sf4/p53* morphants compared to control embryos (std-MO) in gastrulation (80% epiboly). Vertical bars represent standard errors calculated among triplicate reactions.

5. DISCUSSION

In agreement with the previous studies [26], we observed that during zebrafish development *tm9sf4* was expressed starting from fertilization to 5 dpf, suggesting that the expression is both maternal and zygotic (Figure 16). Furthermore, these studies suggested that the gene is ubiquitously expressed in zebrafish adult tissues and has a role in innate immunity signaling [26]. We demonstrated by WISH that *tm9sf4* was mainly expressed in the central nervous system (CNS) during all the analyzed stages (24 hpf, 48 hpf, 72 hpf) and, in particular, in the telencephalon, mesencephalon and cerebellum. Additionally, a marked expression of *tm9sf4* was detected at the eye level, both in retina and crystalline lens (Figure 17). Interestingly, histological sections of the stained embryos showed that the gene was mostly expressed in the periventricular regions of the diencephalon and mesencephalon (Figures 18-20).

To investigate Tm9sf4 protein function during embryonic development, loss-of-function experiments were performed by the injection of two different antisense morpholino oligonucleotides (MOs): a translation-blocking and a splicing morpholino. The translation blocking oligonucleotide (tm9sf4-MO) was designed to target the transcript in the region of the starting codon AUG. Injection of tm9sf4-MO caused severe defects in the central nervous system and a very low survival of the morphants. Co-injecting tm9sf4-MO and an oligo targeting *p53* (p53-MO), the CNS defects were reduced and the survival increased, suggesting that the defects produced by the injection of tm9sf4-MO alone were due to off-target effects. In fact, some morpholinos showed activation of a *p53*-dependent cell death pathway in a sequence-dependent manner, inducing the transcription of a N-terminal truncated *p53* isoform, that uses a recently recognized internal

promoter [48]. Hence, in all the successive experiments we co-injected tm9sf4-MO with p53-MO.

The splicing morpholino (tm9I3E4-MO) was targeted to the junction between intron 3 and exon 4, in order to produce an alternative splicing, resulting in the skipping of exon 4 and in the deletion of a transmembrane domain with consequent overturning of the protein membrane topology. In these conditions, the resulting protein is expected to have an altered functionality.

Following tm9sf4-MO/p53-MO injection, 24 hpf embryos displayed necrosis in the head and a consistent tail bending (Figure 24). Additionally, the brain compartmentalization was not as well defined as in control embryos. At 48 hpf the morphants displayed also cardiac edema and some problems in blood flow; defects persisting up to 72 hpf.

These results were substantially confirmed by tm9I3E4-MO injection (Figure 28). At 24 hpf, the most evident defect of the tm9I3E4-MO injected embryos was a marked tail bending. In particular, we observed defects in the region of the intermediate cell mass (ICM), the site where primitive hematopoiesis and vessels development occur. We could detect a slight necrosis in the head, although the CNS was most strongly affected by tm9sf4-MO/p53-MO injection. At 48 hpf, the necrosis in the head was significantly reduced, while the defects in the tail persisted. Furthermore, in the majority of the morphants the circulation was either not complete or totally absent and some of them displayed cardiac edema or blood stasis in the tail, as in the case of tm9sf4-MO/p53-MO injection.

Since the *tm9sf4* gene was expressed in the central nervous system and protein downregulation caused both necrosis in the head and a reduced brain structure definition, we hypothesized that Tm9sf4 protein has a role in CNS development. Therefore, we analyzed the expression of specific brain

markers in the morphants, to individuate the brain sub-structures that are affected by Tm9sf4 protein downregulation. We selected a set of genes that are representative markers of specific structures of the central nervous system (*fgf8, shha, wnt1, otx2, otx3,* and *krox20*). All the analyzed markers were detected in *tm9sf4* morphants, but had diffuse signals and the brain regions were less defined in our morphants compared to control embryos. Moreover, the midbrain-hindbrain boundary (MHB) was thicker and both *fgf8* and *wnt1* appeared upregulated in *tm9sf4* morphants than in control embryos (Figure 29). This result was confirmed by qRT-PCR on mRNA from 24 hpf morphants, which showed that *fgf8, shha, wnt1* and *otx3* (*otx1a*) were upregulated in *tm9sf4* morphants compared to control embryos, whereas the expression levels of *otx2* and *krox20* (egr1a) were lower in tm9sf4-MO than in std-MO injected embryos (Figure 30).

This result is consistent with the literature about the pathways involved in zebrafish brain development [50], [51], [52]. For example, *fgf8* expression is closely associated with tissues expressing *shh* and *bmp4* and they function together in the patterning of regions of the embryonic head. In particular, *fgf8* regulates regionalization of the prosencephalon through inhibition of *otx2* and *emx2* [53]. Furthermore, the genetic hierarchy of gene expression at the MHB involves multiple positive and negative regulatory loops that result in the establishment of non-overlapping domains of *wnt1* and *fgf8* on either side of the boundary and the consequent specification of the cerebellum. Both *wnt1* and *fgf8* are necessary for the development of the posterior midbrain and cerebellum [54], [55]. *Wnt1* regulates the genetic network, including *otx2*, required for the control of the identity and fate of midbrain dopaminergic progenitors [50]. Moreover, *wnt1* is expressed in a distinct population of boundary cells that forms at the interface of the segments in the zebrafish hindbrain. *Wnt1* knockdown leads to ectopic

expression of boundary cell markers in non-boundary regions of the hindbrain [56].

These results were confirmed by injection of tm9I3E4-MO (Figure 31), with the exception of *krox20*, which was significantly up-regulated in *tm9I3E4* morphants, while it was downregulated in *tm9sf4* morphants, and *otx3*, which underwent a stronger upregulation in *tm9sf4/p53* morphants with respect to *tm9I3E4* morphants (Figures 30 and 31).

In addition to the defects observed in the CNS, loss-of-function experiments showed that protein downregulation caused defects in the ICM region and, at 48 hpf, in the majority of the morphants the circulation was significantly impaired, with some of them displaying cardiac edema or blood stasis in the tail.

This finding was confirmed by loss-of-function experiments on the double transgenic line tg(gata1:dsRed)^{sd2}/tg(flk1:EGFP)^{S843}, which allows the visualization through fluorescence microscopy of both vessel endothelium and circulating erythrocytes. In the majority of the morphants the tail was bent and the circulation was absent, although the tail did not have significant morphological defects. This class of morphants reported defects at the intersomitic vessels (Figure 34), which are formed by angiogenesis.

Interestingly, it was suggested that angiogenesis is a paradigm for many processes including tissue branching, sprouting and cell migration [25]. Thereby, investigating a possible role of *tm9sf4* in angiogenesis may allow us to clarify the protein function in cell migration and branching. It will be necessary to establish whether the circulation problems are caused by defects in the heart development or rather the cardiac edema is due to the defective intersomitic vessels.

Additionally, we found that *tm9sf4* gene was differentially expressed in LA7 cancer stem cells (CSC) with respect to LA7 elongated cells. We

demonstrated that *tm9sf4* downregulation by RNA interference resulted in important changes in LA7 CSC morphology, inducing a trans-differentiation of the CSCs themselves or descendent lineage cells into mesenchymal-like cells, as suggested by the up-regulation of EMT-associated markers by siRNA treatment. Therefore, we hypothesized that the gene is involved in EMT process.

Since it has been shown that many signaling pathways induce EMT in both embryonic development and in normal and transformed cells [27], [44], we wanted to investigate the involvement of *tm9sf4* gene in EMT during zebrafish embryonic development.

Interestingly, according to our previous hypothesis, in zebrafish embryos, the gene was found to be most strongly expressed in periventricular regions of the diencephalon and mesencephalon, where there are proliferating cells that are going to migrate and could undergo epithelial to mesenchymal transition.

Moreover, we observed that the EMT markers found to be upregulated in LA7 cells had conserved sequences and functions in zebrafish. We identified two orthologues for mammal *twist1* (*twist1a* and *twist1b*), two for *zeb2* (*zeb2a* and *zeb2b*) and one for *twist2*.

At 24 hpf, *tm9sf4* downregulation by morpholino injection leaded to an increase of the expression level of *twist2* and *zeb2*, whereas *twist1* expression was not sensibly affected (Figure 32), similarly as observed in LA7 cells, supporting that the gene could have a role in inhibiting EMT processes occurring during embryonic development. This is in contrast with that observed after *tm9sf4* downregulation during zebrafish gastrulation (80% epiboly), in which all EMT markers, except for *zeb2*, did not show a change in expression (Figure 33). However, previous studies suggested that *twist* is not crucial for EMT events associated to gastrulation and that *snail* may be the principal effector [27].

Therefore, since *tm9sf4* downregulation did not result in the change of the EMT markers tested except for *zeb2*, it may not act on these markers to regulate EMT during gastrulation.

Studying the pathways involved in development is difficult due to the complex hierarchy of the components involved in these systems; in particular, many feedback and feedforward loops are involved in embryonic EMT-associated processes. Analysis is also complicated by the fact that the gene expression studies are mostly carried out by *in situ* hybridization, which does not reveal the onset of gene expression, since it requires a sufficient amount of RNA for detection, and when the gene product reaches a concentration sufficient to produce physiological effects. Moreover, generally the expression levels of hundreds of genes change in response to experimental and genetic perturbations [57]. Hence, determining in which order the genes are expressed or repressed becomes a very challenging issue.

Notably, at cellular level, pathological EMTs are very similar to physiological EMTs: they are regulated by the same signaling pathways, regulators and effector molecules [27]. Some of the most known components of signaling pathways involved in embryogenesis are reported in table 6.

All the pathways, regarding both development and tumor progression, converge on E-cadherin regulation. Functional loss of E-cadherin in an epithelial cell has been considered a hallmark of EMT. Some zinc-finger transcription factors were found to directly bind the E-box elements of the E-cadherin promoter and repress its transcription, thereby causing the loss of cell-cell adhesion. These factors include, among others, Snail [39] and ZEB family transcription factors ZEB1 (δEF1) [40], [58] and ZEB2 (SIP1) [41]. These factors are capable of suppressing critical components that contribute to set up of the epithelial phenotype. For instance, recently,

ZEB1, Snail and Slug were reported to repress the transcription of polarity factors, including *Crumbs3* and *Lgl2* [58]. These transcription factors are involved in various EMT processes during embryogenesis (Table 6).

Developmental process	TGF-β pathway	Wnt pathway	Notch pathway	TK receptors	Transcription factors
Mesoderm formation	Nodal	Canonical Wnt	Not determined	FGFR	Snail
Neural crest migration	TGF-β 1,2,3 BMP	Canonical Wnt Non canonical	Regulate BMP signaling	FGFR PDGFR	Snail, Slug, Twist1, ZEB2
Cardiac valve formation	TGF-β 3	Not determined	Jagged 1 Notch 1	ErbB3	Not determined

Table 6 EMT-associated signaling pathways components involved in embryonic development.

We found *zeb2* to be upregulated following *tm9sf4* knock down both in LA7 cell line, used as a model of mammary gland cancer stem cells, and during zebrafish embryonic development, suggesting that *tm9sf4* downregulation cause an increase of *zeb2* expression level and consequent E-cadherin transcription repression mediated by *zeb2*, leading to the loss of cell-cell adhesion and promoting EMT. Therefore, *tm9sf4* could negatively regulate EMT during zebrafish neurulation, by promoting cell-cell adhesion.

In zebrafish, the anterior neurocranium is derived from the anterior cranial neural crest cells, which migrate from the dorsal neural tube and reach the head, following a path along the optic stalks, medial to the eyes. Migration begins at 12 hpf and by 15 hpf the cells moves into pharyngeal arches. Successively, neural crest cells migrate around the eye, where they cannot be detected until 24 hpf.

Therefore, the changes in expression of EMT markers suggest that *tm9sf4* expression inhibits EMT during neurulation.

In our study, *twist1* expression level was not affected by Tm9sf4 protein downregulation at both 24 hpf and 80% epiboly.

Twist1 [43], [59] and Goosecoid, known as the Spemann organizer gene [60], induce EMT in certain epithelial cells through E-cadherin repression, although they are not able to directly bind to E-cadherin promoter. *Twist1* have been found to be capable of inducing EMT in human mammary epithelial cells [42]. In vertebrates, it is mainly expressed in neural crest cells [43] and it is required for migration and differentiation of neural crest and head mesenchymal cells in mice [59].

We demonstrated that in 80% epiboly embryos, following *tm9sf4* downregulation, *zeb2* was downregulated, while other markers were unaffected. This result is in contrast with our previous findings on LA7 cells, suggesting that *tm9sf4* may not function through these markers or that *tm9sf4,* rather than inhibiting, promotes EMT during zebrafish gastrulation.

However, according to our previous hypothesis, we demonstrated that Tm9sf4 protein downregulation induces a decrease of the E-cadherin expression level during gastrulation (Figure 34), suggesting that it promotes the loss of cell-cell adhesion. Further investigations will allow us to better clarify this issue. For instance, protein staining of *zeb2* and other EMT associated proteins will allow us to detect which cells in which substructures of tissue display changes in expression with *tm9sf4* down regulation.

All the aforementioned factors are able to repress E-cadherin directly or indirectly. However, it is not clear how they are involved in EMT-associated cell behaviors, including mesenchymal trans-differentiation, cell motility and invasion. In fact, E-cadherin repressors function as complete and self-sufficient EMT inducers, regulating the expression of genes that repress the epithelial character and promote the mesenchymal state. In addition, they induce the loss of epithelial cell polarity and cell division, whereas promote

cell survival. The EMT inducers that indirectly repress E-cadherin transcription frequently activate some of the direct repressors and they also act on multiple targets.

For example, it has been demonstrated that *snail1* [61]*, zeb1* [58] and *TGF-*β alter epithelial cell polarity by repressing the transcription of components belonging to the complexes involved in the maintaining of apicobasal polarity (Par, Crumbs, Scribble). Moreover, Snail and ZEB factors induce the expression of metalloproteases that degrade the basement membrane, some of which are sufficient to induce EMT, by triggering a positive regulatory feedback loop [62]. However, both in development and in carcinoma progression, *snail1* is expressed at the onset of the transition, whereas *snail2*, ZEB genes and *twist* are successively induced to maintain the migratory mesenchymal state [63].

An additional attractive pathway is the β-catenin-mediated transcription program. The loss of E-cadherin from adherent junctions causes the release into the cytoplasm of β–catenin, which enters the nucleus and activate transcription of factors including *slug* [64] and *twist1* [65], thereby contributing to the EMT program.

In addition to E-cadherin, N-cadherin-mediated adhesion plays an important role in neural crest associated EMT, where N-cadherin and cadherin 6 downregulation occurs as well as expression of the less adhesive type II cadherins, including cadherin 7 and 11 [66].

The role of *tm9sf4* has not been explored in this context. Investigating whether *tm9sf4* influences other components of the EMT signaling pathways acting during zebrafish development will allow us in the future to clarify its role in this process.

It is interesting to consider that several studies reported that *tm9sf4* could be involved in cell adhesion both in *Dictyostelium* [1] and *Drosophila* plasmatocytes [3], [4]. In addition, it has been recently proposed that

tm9sf4 hypoxia-mediated downregulation induces a decrease of cell adhesion in leukemic cells to fibronectin [67]. All of these studies support our hypothesis that *tm9sf4* has a role in cell-cell contact.

6. CONCLUSIONS

According to previous findings [26], we found that during zebrafish embryonic development *tm9sf4* was expressed in all of the stages from oocytes to 5 dpf, suggesting that the expression is both maternal and zygotic.

Furthermore, the gene was found to be mainly expressed in the brain and loss-of-function analyses by antisense morpholino oligonucleotide injection showed that *tm9sf4* downregulation induced defects in the CNS, which displayed an impaired regionalization.
WISH analysis of specific brain markers (*fgf8, otx2, shha, wnt1)* confirmed that the brain regions targeted by these probes were all formed in *tm9sf4* morphants, but they were less defined with respect to those observed in control embryos; additionally, the midbrain-hindbrain boundary (MHB) appeared thicker in our morphants than in control embryos.
Real Time PCR showed that, as expected, *tm9sf4* downregulation induced an increase of the expression level of *fgf8, shha, wnt1* and a reduction of *otx2* level. The results regarding the effect of *tm9sf4* downregulation on *krox20* (*egr1a*) and *otx3* (*otx1a*) were controversial.
In situ hybridization for *krox20* and *otx3* will be performed to further investigate this issue. Expression analysis of other markers is now in progress, to better understand the specific regions affected by protein downregulation and, possibly, the pathways in which they are involved. However, these findings suggest a role for *tm9sf4* in zebrafish brain development.

Additionally, *tm9sf4* downregulation caused 24 hpf embryos to have a bent tail, with defects in the ICM region, the site where the primitive hematopoiesis and blood vessels development occur. At 48 hpf the blood

circulation was significantly affected by protein downregulation and embryos reported cardiac edema and blood stasis in the tail, in addition to morphological defects in the intersomitic vessels, which are formed by angiogenesis. Interestingly, it was suggested that angiogenesis represents a paradigm for many core biological processes such as tissue morphogenesis through branching, cell migration and lumen formation, all of which are involved in the morphogenesis of many other organs [25].
It will be necessary to establish whether the circulation problems are caused by defects in the heart development or rather the cardiac edema is due to the defective intersomitic vessels. At this purpose, both expression analysis of cardiac markers, following protein downregulation, and loss-of-function experiments, using specific transgenic lines, will be carried out.

Our previous studies showed that *tm9sf4* gene was more strongly expressed in LA7 cancer stem cells with respect to LA7 elongated cells. *Tm9sf4* downregulation by RNA interference resulted in important changes in LA7 CSC morphology, inducing them to trans-differentiate to mesenchymal-like cells. According to these results, we demonstrated that the expression of EMT-associated markers by LA7 cells increased following *tm9sf4* downregulation.
Based on the foundation that cellular processes and signaling pathways governing EMT are conserved in embryogenesis and tumor progression, we proposed that *tm9sf4* is involved in EMT processes occurring during zebrafish embryonic development.
We demonstrated that *tm9sf4* downregulation induced an increase of *zeb2* and *twist2* expression level by 24 hpf embryos, suggesting that *tm9sf4* induces negative regulation of these factors, inhibiting E-cadherin transcriptional repression and thereby promoting cell-cell adhesion. This hypothesis is consistent with previous studies, which proposed a role of

tm9sf4 in cell adhesion [1], [3], [4], [67]. Therefore, *tm9sf4* could be involved in repressing EMT during zebrafish neurulation.

In accordance to this hypothesis, we demonstrated that Tm9sf4 protein downregulation induced a decrease of E-cadherin expression level during gastrulation, which could promote the loss of cell-cell adhesion.

Interestingly, the gene was found to be mainly expressed in periventricular regions of the diencephalon and mesencephalon, where there are proliferating cells that are going to migrate and could undergo epithelial to mesenchymal transition.

In the near future we are going to further investigate this issue by determining in which specific CNS cells the gene is expressed and by studying *tm9sf4* effect on the expression of other components of the EMT signaling pathways, including Wnt signaling, TGF-β (BMP, Nodal), Snail and E-cadherin, both in zebrafish gastrulation and neurulation.

7. **REFERENCES**

[1] S. Cornillon, E. Pech, M. Benghezal, K. Ravanel, E. Gaynor, F. Letourneur, F. Brückert, and P. Cosson, “Phg1p is a nine-transmembrane protein superfamily member involved in dictyostelium adhesion and phagocytosis.,” *J. Biol. Chem.*, vol. 275, no. 44, pp. 34287–92, Nov. 2000.

[2] F. Lozupone, M. Perdicchio, D. Brambilla, M. Borghi, S. Meschini, S. Barca, M. L. Marino, M. Logozzi, C. Federici, E. Iessi, A. de Milito, and S. Fais, “The human homologue of Dictyostelium discoideum phg1A is expressed by human metastatic melanoma cells.,” *EMBO Rep.*, vol. 10, no. 12, pp. 1348–54, Dec. 2009.

[3] E. Bergeret, J. Perrin, M. Williams, D. Grunwald, E. Engel, D. Thevenon, E. Taillebourg, F. Bruckert, P. Cosson, and M.-O. Fauvarque, “TM9SF4 is required for Drosophila cellular immunity via cell adhesion and phagocytosis.,” *J. Cell Sci.*, vol. 121, no. Pt 20, pp. 3325–34, Oct. 2008.

[4] M.-O. Fauvarque and M. J. Williams, “Drosophila cellular immunity: a story of migration and adhesion,” *J. Cell Sci.*, vol. 124, no. 9, pp. 1373–1382, 2011.

[5] L. Lugini, P. Matarrese, A. Tinari, F. Lozupone, C. Federici, E. Iessi, M. Gentile, F. Luciani, G. Parmiani, L. Rivoltini, W. Malorni, and S. Fais, “Cannibalism of live lymphocytes by human metastatic but not primary melanoma cells.,” *Cancer Res.*, vol. 66, no. 7, pp. 3629–38, Apr. 2006.

[6] S. Fais and M.-O. Fauvarque, “TM9 and cannibalism: how to learn more about cancer by studying amoebae and invertebrates.,” *Trends Mol. Med.*, vol. 18, no. 1, pp. 4–5, Jan. 2012.

[7] S. Fais, “Cannibalism: a way to feed on metastatic tumors.,” *Cancer Lett.*, vol. 258, no. 2, pp. 155–64, Dec. 2007.

[8] L. Lugini, F. Lozupone, P. Matarrese, C. Funaro, F. Luciani, W. Malorni, L. Rivoltini, C. Castelli, A. Tinari, A. Piris, G. Parmiani, and S. Fais, "Potent Phagocytic Activity Discriminates Metastatic and Primary Human Malignant Melanomas: A Key Role of Ezrin," *Lab. Investig.*, vol. 83, no. 11, pp. 1555–1567, 2003.

[9] R. Dulbecco, M. Bologna, and M. Unger, "Role of Thy-1 antigen in the in vitro differentiation of a rat mammary cell line.," *Proc. Natl. Acad. Sci. U. S. A.*, vol. 76, no. 4, pp. 1848–1852, 1979.

[10] J. J. Going, H. M. Abd El-Monem, and J. a Craft, "Clonal origins of human breast cancer," *J Pathol*, vol. 194, no. 4, pp. 406–412, 2001.

[11] I. Zucchi, S. Sanzone, S. Astigiano, P. Pelucchi, M. Scotti, V. Valsecchi, O. Barbieri, G. Bertoli, a Albertini, R. a Reinbold, and R. Dulbecco, "The properties of a mammary gland cancer stem cell.," *Proc. Natl. Acad. Sci. U. S. A.*, vol. 104, no. 25, pp. 10476–81, Jun. 2007.

[12] C. Cocola, S. Sanzone, S. Astigiano, P. Pelucchi, E. Piscitelli, L. Vilardo, O. Barbieri, G. Bertoli, R. a Reinbold, and I. Zucchi, "A rat mammary gland cancer cell with stem cell properties of self-renewal and multi-lineage differentiation.," *Cytotechnology*, vol. 58, no. 1, pp. 25–32, Sep. 2008.

[13] I. Zucchi, S. Astigiano, G. Bertalot, S. Sanzone, C. Cocola, P. Pelucchi, G. Bertoli, M. Stehling, O. Barbieri, a Albertini, H. R. Schöler, B. G. Neel, R. a Reinbold, and R. Dulbecco, "Distinct populations of tumor-initiating cells derived from a tumor generated by rat mammary cancer stem cells.," *Proc. Natl. Acad. Sci. U. S. A.*, vol. 105, no. 44, pp. 16940–5, Nov. 2008.

[14] J. F. Amatruda, J. L. Shepard, H. M. Stern, and L. I. Zon, "Zebrafish as a cancer model system.," *Cancer Cell*, vol. 1, no. 3, pp. 229–31, Apr. 2002.

[15] N. D. Meeker and N. S. Trede, "Immunology and zebrafish: spawning new models of human disease.," *Dev. Comp. Immunol.*,

vol. 32, no. 7, pp. 745–57, Jan. 2008.

[16] K. Dooley and L. I. Zon, “Zebrafish: a model system for the study of human disease.,” *Curr. Opin. Genet. Dev.*, vol. 10, no. 3, pp. 252–6, Jun. 2000.

[17] C. Sullivan and C. H. Kim, “Zebrafish as a model for infectious disease and immune function.,” *Fish Shellfish Immunol.*, vol. 25, no. 4, pp. 341–50, Oct. 2008.

[18] Z. Lele and P. H. Krone, “The zebrafish as a model system in developmental, toxicological and transgenic research,” *Biotechnol. Adv.*, vol. 14, no. 1, pp. 57–72, Jan. 1996.

[19] R. M. White, A. Sessa, C. Burke, T. Bowman, J. LeBlanc, C. Ceol, C. Bourque, M. Dovey, W. Goessling, C. E. Burns, and L. I. Zon, “Transparent Adult Zebrafish as a Tool for In Vivo Transplantation Analysis,” *Cell Stem Cell*, vol. 2, no. 2, pp. 183–189, 2008.

[20] G. J. Lieschke, a C. Oates, M. O. Crowhurst, a C. Ward, and J. E. Layton, “Morphologic and functional characterization of granulocytes and macrophages in embryonic and adult zebrafish.,” *Blood*, vol. 98, no. 10, pp. 3087–3096, 2001.

[21] J. R. Goldsmith and C. Jobin, “Think Small: Zebrafish as a Model System of Human Pathology,” *J. Biomed. Biotechnol.*, vol. 2012, pp. 1–12, 2012.

[22] H. W. Detrich, M. W. Kieran, F. Y. Chan, L. M. Barone, K. Yee, J. a Rundstadler, S. Pratt, D. Ransom, and L. I. Zon, “Intraembryonic hematopoietic cell migration during vertebrate development.,” *Proc. Natl. Acad. Sci. U. S. A.*, vol. 92, no. 23, pp. 10713–7, 1995.

[23] G. R. Dressler, “Kidney development branches out.,” *Dev. Genet.*, vol. 24, no. 3–4, pp. 189–93, 1999.

[24] R. T. Peterson, B. a Link, J. E. Dowling, and S. L. Schreiber, “Small

molecule developmental screens reveal the logic and timing of vertebrate development.," *Proc. Natl. Acad. Sci. U. S. A.*, vol. 97, no. 24, pp. 12965–9, 2000.

[25] S. P. Herbert and D. Y. R. Stainier, "Molecular control of endothelial cell behaviour during blood vessel morphogenesis," *Nat. Rev. Mol. Cell Biol.*, vol. 12, no. 9, pp. 551–564, 2011.

[26] B. Pruvot, V. Laurens, F. Salvadori, E. Solary, L. Pichon, and J. Chluba, "Comparative analysis of nonaspanin protein sequences and expression studies in zebrafish.," *Immunogenetics*, vol. 62, no. 10, pp. 681–99, Oct. 2010.

[27] J. P. Thiery, H. Acloque, R. Y. J. Huang, and M. A. Nieto, "Epithelial-Mesenchymal Transitions in Development and Disease," *Cell*, vol. 139, no. 5, pp. 871–890, 2009.

[28] L. Solnica-Krezel, "Gastrulation in zebrafish — all just about adhesion?," *Curr. Opin. Genet. Dev.*, vol. 16, no. 4, pp. 433–441, 2006.

[29] a. Barrallo-Gimeno, "The Snail genes as inducers of cell movement and survival: implications in development and cancer," *Development*, vol. 132, no. 14, pp. 3151–3161, 2005.

[30] Y. Nakaya, E. W. Sukowati, Y. Wu, and G. Sheng, "RhoA and microtubule dynamics control cell–basement membrane interaction in EMT during gastrulation," *Nat. Cell Biol.*, vol. 10, no. 7, pp. 765–775, 2008.

[31] J. Egea, C. Erlacher, E. Montanez, I. Burtscher, S. Yamagishi, M. Heß, F. Hampel, R. Sanchez, M. T. Rodriguez-manzaneque, M. R. Bösl, R. Fässler, H. Lickert, and R. Klein, "Genetic ablation of FLRT3 reveals a novel morphogenetic function for the anterior visceral endoderm in suppressing mesoderm differentiation," pp. 3349–3362, 2008.

[32] T. Shimizu, T. Yabe, O. Muraoka, S. Yonemura, S. Aramaki, K. Hatta, Y. K. Bae, H. Nojima, and M. Hibi, "E-cadherin is required for gastrulation cell movements in zebrafish," *Mech. Dev.*, vol. 122, no. 6, pp. 747–763, 2005.

[33] D. a. Kane, "Mutations in half baked/E-cadherin block cell behaviors that are necessary for teleost epiboly," *Development*, vol. 132, no. 5, pp. 1105–1116, 2005.

[34] S. Yamashita, C. Miyagi, T. Fukada, N. Kagara, Y.-S. Che, and T. Hirano, "Zinc transporter LIVI controls epithelial-mesenchymal transition in zebrafish gastrula organizer.," *Nature*, vol. 429, no. 6989, pp. 298–302, 2004.

[35] F. Ulrich, M. Krieg, E.-M. Schötz, V. Link, I. Castanon, V. Schnabel, A. Taubenberger, D. Mueller, P.-H. Puech, and C.-P. Heisenberg, "Wnt11 Functions in Gastrulation by Controlling Cell Cohesion through Rab5c and E-Cadherin," *Dev. Cell*, vol. 9, no. 4, pp. 555–564, 2005.

[36] F. Lin, "Essential roles of G 12/13 signaling in distinct cell behaviors driving zebrafish convergence and extension gastrulation movements," *J. Cell Biol.*, vol. 169, no. 5, pp. 777–787, 2005.

[37] N. S. Glickman, C. B. Kimmel, M. a Jones, and R. J. Adams, "Shaping the zebrafish notochord.," *Development*, vol. 130, no. 5, pp. 873–887, 2003.

[38] C. Carmona-Fontaine, H. K. Matthews, S. Kuriyama, M. Moreno, G. a Dunn, M. Parsons, C. D. Stern, and R. Mayor, "Contact inhibition of locomotion in vivo controls neural crest directional migration.," *Nature*, vol. 456, no. 7224, pp. 957–61, 2008.

[39] E. Batlle, E. Sancho, C. Francí, D. Domínguez, M. Monfar, J. Baulida, and a García De Herreros, "The transcription factor snail is a repressor of E-cadherin gene expression in epithelial tumour cells.," *Nat. Cell Biol.*, vol. 2, no. 2, pp. 84–89, 2000.

[40] A. Eger, K. Aigner, S. Sonderegger, B. Dampier, S. Oehler, M. Schreiber, G. Berx, A. Cano, H. Beug, and R. Foisner, “DeltaEF1 is a transcriptional repressor of E-cadherin and regulates epithelial plasticity in breast cancer cells,” *Oncogene*, vol. 24, no. 14, pp. 2375–2385, 2005.

[41] J. Comijn, G. Berx, P. Vermassen, K. Verschueren, L. Van Grunsven, E. Bruyneel, M. Mareel, D. Huylebroeck, and F. Van Roy, “The two-handed E box binding zinc finger protein SIP1 downregulates E-cadherin and induces invasion,” *Mol. Cell*, vol. 7, no. 6, pp. 1267–1278, 2001.

[42] J. Yang, S. A. Mani, J. L. Donaher, S. Ramaswamy, R. A. Itzykson, C. Come, P. Savagner, I. Gitelman, A. Richardson, R. A. Weinberg, C. Val, and A. Lamarque, “Twist , a Master Regulator of Morphogenesis , Plays an Essential Role in Tumor Metastasis Ben Gurion University of the Negev,” vol. 117, pp. 927–939, 2004.

[43] I. Gitelman, “Twist protein in mouse embryogenesis.,” *Dev. Biol.*, vol. 189, no. 2, pp. 205–214, 1997.

[44] J. Yang and R. a. Weinberg, “Epithelial-Mesenchymal Transition: At the Crossroads of Development and Tumor Metastasis,” *Dev. Cell*, vol. 14, no. 6, pp. 818–829, 2008.

[45] C. B. Kimmel, W. W. Ballard, S. R. Kimmel, B. Ullmann, and T. F. Schilling, “Stages of embryonic development of the zebrafish.,” *Dev. Dyn.*, vol. 203, no. 3, pp. 253–310, Jul. 1995.

[46] M. M. Santoro, T. Samuel, T. Mitchell, J. C. Reed, and D. Y. R. Stainier, “Birc2 (cIap1) regulates endothelial cell integrity and blood vessel homeostasis.,” *Nat. Genet.*, vol. 39, no. 11, pp. 1397–402, Nov. 2007.

[47] C. Thisse, B. Thisse, T. F. Schilling, and J. H. Postlethwait, “Structure of the zebrafish snail1 gene and its expression in wild-type, spadetail and no tail mutant embryos.,” *Development*, vol. 119, no. 4, pp. 1203–1215, 1993.

[48] M. E. Robu, J. D. Larson, A. Nasevicius, S. Beiraghi, C. Brenner, S. a Farber, and S. C. Ekker, "P53 Activation By Knockdown Technologies.," *PLoS Genet.*, vol. 3, no. 5, p. e78, May 2007.

[49] a Nasevicius and S. C. Ekker, "Effective targeted gene 'knockdown' in zebrafish.," *Nat. Genet.*, vol. 26, no. 2, pp. 216–220, 2000.

[50] N. Prakash, C. Brodski, T. Naserke, E. Puelles, R. Gogoi, A. Hall, M. Panhuysen, D. Echevarria, L. Sussel, D. M. V. Weisenhorn, S. Martinez, E. Arenas, A. Simeone, and W. Wurst, "A Wnt1-regulated genetic network controls the identity and fate of midbrain-dopaminergic progenitors in vivo.," *Development*, vol. 133, no. 1, pp. 89–98, 2006.

[51] B. T. Phillips, K. Bolding, and B. B. Riley, "Zebrafish fgf3 and fgf8 encode redundant functions required for otic placode induction.," *Dev. Biol.*, vol. 235, no. 2, pp. 351–365, 2001.

[52] C. Y. Su, H. a. Kemp, and C. B. Moens, "Cerebellar development in the absence of Gbx function in zebrafish," *Dev. Biol.*, vol. 386, no. 1, pp. 181–190, 2014.

[53] P. H. Crossley, S. Martinez, Y. Ohkubo, and J. L. R. Rubenstein, "Coordinate expression of Fgf8, Otx2, Bmp4, and Shh in the rostral prosencephalon during development of the telencephalic and optic vesicles," *Neuroscience*, vol. 108, no. 2, pp. 183–206, 2001.

[54] S. K. Sgaier, S. Millet, M. P. Villanueva, F. Berenshteyn, C. Song, and A. L. Joyner, "Morphogenetic and cellular movements that shape the mouse cerebellum: Insights from genetic fate mapping," *Neuron*, vol. 45, no. 1, pp. 27–40, 2005.

[55] C. L. Chi, S. Martinez, W. Wurst, and G. R. Martin, "The isthmic organizer signal FGF8 is required for cell survival in the prospective midbrain and cerebellum.," *Development*, vol. 130, no. 12, pp. 2633–2644, 2003.

[56] M. Amoyel, Y.-C. Cheng, Y.-J. Jiang, and D. G. Wilkinson, “Wnt1 regulates neurogenesis and mediates lateral inhibition of boundary cell specification in the zebrafish hindbrain.,” *Development*, vol. 132, no. 4, pp. 775–785, 2005.

[57] M. Klymkowsky, C. Cortez Rossi, and K. B. Artinger, “Mechanisms driving neural crest induction and migration in the zebrafish and Xenopus laevis,” *Cell Adh. Migr.*, vol. 4, no. 4, pp. 595–608, Oct. 2010.

[58] S. Spaderna, O. Schmalhofer, M. Wahlbuhl, a. Dimmler, K. Bauer, a. Sultan, F. Hlubek, a. Jung, D. Strand, a. Eger, T. Kirchner, J. Behrens, and T. Brabletz, “The Transcriptional Repressor ZEB1 Promotes Metastasis and Loss of Cell Polarity in Cancer,” *Cancer Res.*, vol. 68, no. 2, pp. 537–544, 2008.

[59] K. Soo, M. P. O’Rourke, P.-L. Khoo, K. a Steiner, N. Wong, R. R. Behringer, and P. P. L. Tam, “Twist function is required for the morphogenesis of the cephalic neural tube and the differentiation of the cranial neural crest cells in the mouse embryo.,” *Dev. Biol.*, vol. 247, no. 2, pp. 251–270, 2002.

[60] K. A. Hartwell, B. Muir, F. Reinhardt, A. E. Carpenter, D. C. Sgroi, and R. A. Weinberg, “The Spemann organizer gene, Goosecoid, promotes tumor metastasis.,” *Proc. Natl. Acad. Sci. U. S. A.*, vol. 103, no. 50, pp. 18969–74, 2006.

[61] E. L. Whiteman, C.-J. Liu, E. R. Fearon, and B. Margolis, “The transcription factor snail represses Crumbs3 expression and disrupts apico-basal polarity complexes,” *Oncogene*, vol. 27, no. 27, pp. 3875–3879, 2008.

[62] D. C. Radisky, D. D. Levy, L. E. Littlepage, H. Liu, C. M. Nelson, J. E. Fata, D. Leake, E. L. Godden, D. G. Albertson, M. Angela Nieto, Z. Werb, and M. J. Bissell, “Rac1b and reactive oxygen species mediate MMP-3-induced EMT and genomic instability,” *Nature*, vol. 436, no. 7047, pp. 123–127, 2005.

[63] H. Peinado, D. Olmeda, and A. Cano, “Snail, Zeb and bHLH factors in tumour progression: an alliance against the epithelial phenotype?,” *Nat. Rev. Cancer*, vol. 7, no. 6, pp. 415–428, 2007.

[64] M. Conacci-Sorrell, I. Simcha, T. Ben-Yedidia, J. Blechman, P. Savagner, and A. Ben-Ze’Ev, “Autoregulation of E-cadherin expression by cadherin-cadherin interactions: The roles of β-catenin signaling, Slug, and MAPK,” *J. Cell Biol.*, vol. 163, no. 4, pp. 847–857, 2003.

[65] T. T. Onder, P. B. Gupta, S. A. Mani, J. Yang, E. S. Lander, and R. A. Weinberg, “Loss of E-Cadherin Promotes Metastasis via Multiple Downstream Transcriptional Pathways,” *Cancer Res.*, vol. 68, no. 10, pp. 3645–3654, 2008.

[66] J. Vallin, J. M. Girault, J. P. Thiery, and F. Broders, “Xenopus cadherin-11 is expressed in different populations of migrating neural crest cells,” *Mech. Dev.*, vol. 75, pp. 171–174, 1998.

[67] R. Paolillo, I. Spinello, M. T. Quaranta, L. Pasquini, E. Pelosi, F. Lo Coco, U. Testa, and C. Labbaye, “Human TM9SF4 Is a New Gene Down-Regulated by Hypoxia and Involved in Cell Adhesion of Leukemic Cells,” *PLoS One*, vol. 10, no. 5, p. e0126968, 2015.

ACKNOWLEDGEMENTS

First of all, I wish to express my deepest gratitude to my supervisor, ***Dr. Ileana Zucchi*** *(CNR-ITB, Segrate), for her expert guidance and aid throughout my study.*

A very special thank you to ***Dr. Paride Pelucchi*** *for helping me with my research and being a constant source of motivation. Thanks a lot for everything.*

I am extremely grateful to my friend, ***Dr. Stefano Molgora****, for the support he has lent me over all these years.*

I also thank ***Dr. Rolland Reinbold*** *for his time and effort in checking this manuscript,* ***Laura Vilardo*** *for the preliminary data and the other members of my group.*

In addition, I would like to express my sincere gratitude to ***Professor Franco Cotelli*** *(Department of Bioscience, University of Milan) for providing me with all the necessary facilities,* ***Dr. Silvia Carra****, whose technical expertise, knowledge and time were generously shared, and all the members of the lab.*

I also thank my tutor ***Cristina Battaglia*** *for her helpfulness.*

Finally, a thank you to ***my family and friends*** *for their unconditional love. They have always been there for me and I am thankful for everything they have helped me achieve.*

This work was supported by FIRB RBAP11BYNP "Nanosistemi avanzati per una nuova oncologia molecolare" NEWTON.